

HIGH STRAIN RATE TENSILE PROPERTIES OF WELDED DOP-26 IRIDIUM



J. H. Schneibel
R. G. Miller
C. A. Carmichael
E. E. Fox
G. B. Ulrich
E. P. George

August 2017

**Approved for public release.
Distribution is unlimited.**

DOCUMENT AVAILABILITY

Reports produced after January 1, 1996, are generally available free via US Department of Energy (DOE) SciTech Connect.

Website <http://www.osti.gov/scitech/>

Reports produced before January 1, 1996, may be purchased by members of the public from the following source:

National Technical Information Service
5285 Port Royal Road
Springfield, VA 22161
Telephone 703-605-6000 (1-800-553-6847)
TDD 703-487-4639
Fax 703-605-6900
E-mail info@ntis.gov
Website <http://www.ntis.gov/help/ordermethods.aspx>

Reports are available to DOE employees, DOE contractors, Energy Technology Data Exchange representatives, and International Nuclear Information System representatives from the following source:

Office of Scientific and Technical Information
PO Box 62
Oak Ridge, TN 37831
Telephone 865-576-8401
Fax 865-576-5728
E-mail reports@osti.gov
Website <http://www.osti.gov/contact.html>

This report was prepared as an account of work sponsored by an agency of the United States Government. Neither the United States Government nor any agency thereof, nor any of their employees, makes any warranty, express or implied, or assumes any legal liability or responsibility for the accuracy, completeness, or usefulness of any information, apparatus, product, or process disclosed, or represents that its use would not infringe privately owned rights. Reference herein to any specific commercial product, process, or service by trade name, trademark, manufacturer, or otherwise, does not necessarily constitute or imply its endorsement, recommendation, or favoring by the United States Government or any agency thereof. The views and opinions of authors expressed herein do not necessarily state or reflect those of the United States Government or any agency thereof.

Materials Science and Technology Division

**HIGH STRAIN RATE TENSILE PROPERTIES
OF WELDED DOP-26 IRIDIUM**

Authors:

J. H. Schneibel
R. G. Miller
C. A. Carmichael
E. E. Fox
G. B. Ulrich
E. P. George

Date Published: August 2017

Prepared by
OAK RIDGE NATIONAL LABORATORY
Oak Ridge, TN 37831-6283
managed by
UT-BATTELLE, LLC
for the
US DEPARTMENT OF ENERGY
under contract DE-AC05-00OR22725

CONTENTS

CONTENTS	iii
LIST OF FIGURES	v
LIST OF TABLES	vii
ABSTRACT	1
1. INTRODUCTION	1
2. EXPERIMENTAL PROCEDURE.....	2
2.1. WELDING	2
2.2. SPECIMEN FABRICATION	3
2.3. MECHANICAL TESTING.....	5
3. RESULTS AND DISCUSSION.....	7
3.1. MICROSTRUCTURE OF WELDS.....	7
3.2. STRESS-STRAIN CURVES	9
3.3. EVALUATION AND DISCUSSION OF STRESS-STRAIN CURVES	19
3.4. FRACTURE SURFACE OBSERVATIONS	25
4. SUMMARY AND CONCLUSIONS.....	27
5. SUGGESTIONS FOR FURTHER WORK.....	28
6. REFERENCES	29
WELDED IRIIDIUM ALLOY TENSILE TEST SPECIMEN PREPARATION TRAVELER..	A-3

LIST OF FIGURES

Fig. 1.	Drawing of tensile test specimen with machining instructions	4
Fig. 2.	Schematic of stress vs. crosshead strain	6
Fig. 3.	Light microscope image showing the microstructure of the weld region and base metal in a plane parallel to the plane of the blank. During welding, the weld bead progressed from the top to the bottom of the micrograph	7
Fig. 4.	Light microscope image showing the microstructure of the weld region and base metal in a plane perpendicular to the plane of the blank	8
Fig. 5.	Stress-strain curves for welded DOP-26 with MRM heat treatment tested at 10^{-3} s^{-1} and 25°C , (a) full curves, (b) yield region	9
Fig. 6.	Stress-strain curves for welded DOP-26 without MRM heat treatment tested at 10^{-3} s^{-1} and 750°C , (a) full curves, (b) yield region	10
Fig. 7.	Stress-strain curves for welded DOP-26 with MRM heat treatment tested at 10^{-3} s^{-1} and 750°C , (a) full curves, (b) yield region	11
Fig. 8.	Stress-strain curves for welded DOP-26 with MRM heat treatment tested at 10^{-3} s^{-1} and 900°C , (a) full curves, (b) yield region	12
Fig. 9.	Stress-strain curves for welded DOP-26 without MRM heat treatment tested at 10^{-3} s^{-1} and 1090°C , (a) full curves, (b) yield region	13
Fig. 10.	Stress-strain curves for welded DOP-26 with MRM heat treatment tested at 10^{-3} s^{-1} and 1090°C , (a) full curves, (b) yield region	14
Fig. 11.	Stress-strain curves for welded DOP-26 with MRM heat treatment tested at 10 s^{-1} and 25°C , (a) full curves, (b) yield region	15
Fig. 12.	Stress-strain curves for welded DOP-26 with MRM heat treatment tested at 10 s^{-1} and 750°C , (a) full curves, (b) yield region	16
Fig. 13.	Stress-strain curves for welded DOP-26 with MRM heat treatment tested at 10 s^{-1} and 900°C , (a) full curves, (b) yield region	17
Fig. 14.	Stress-strain curves for welded DOP-26 with MRM heat treatment tested at 10 s^{-1} and 1090°C , (a) full curves, (b) yield region	18
Fig. 15.	Yield stress (YS) and ultimate tensile stress (UTS) for welded DOP-26 with MRM heat treatment deformed at a strain rate of $1 \times 10^{-3} \text{ s}^{-1}$. The YS and UTS values for the DOP-26 base material (without MRM heat treatment) from ORNL/TM-2007/81[12] are shown for comparison.....	23
Fig. 16.	Yield stress (YS) and ultimate tensile stress (UTS) for welded DOP-26 with MRM heat treatment deformed at a strain rate of 10 s^{-1} . The YS and UTS values for the DOP-26 base material (without MRM heat treatment) from ORNL/TM-2007/81[12] are shown for comparison.....	23
Fig. 17.	Effect of strain rate on yield stress (YS) and ultimate tensile stress (UTS) of welded DOP-26 with MRM heat treatment	24
Fig. 18.	Fracture strain of welded DOP-26 with MRM heat treatment. The corresponding values for the DOP-26 base material (without MRM heat treatment) are shown for comparison	24
Fig. 19.	Scanning electron microscope image of fracture surface of specimen GR9-3-5-1 tested at room temperature and $1 \times 10^{-3} \text{ s}^{-1}$	25
Fig. 20.	Scanning electron microscope image of fracture surface of specimen GR9-3-7-3 tested at 900°C and $1 \times 10^{-3} \text{ s}^{-1}$	26
Fig. 21.	Light microscope image of a longitudinal cross section (left) and scanning electron micrograph of the fracture surface (right) of specimen AR2-4-6-3 (a non-prime DOP-26 material) tested at 900°C and 10 s^{-1}	26

LIST OF TABLES

Table 1. Welding Parameters.....	2
Table 2. Test Matrix for Tensile Specimens showing the Number of Tests carried out for each Heat Treat Condition/Test Temperature/Strain Rate Combination	5
Table 3. Results of Metallurgical Evaluation of Welds.....	8
Table 4. Fracture Strains, and Slopes of Elastic Lines, for Welded DOP-26	21
Table 5. Fracture Strains, Yield Stresses and Ultimate Tensile Stresses for Welded DOP-26 (Present Study) and DOP-26 Base Material (ORNL/TM-2007/81, Ref [12]).....	22
Table 6. Percentage of Transgranular Failure on Fracture Surfaces of Welded DOP-26 With MRM Heat Treatment.....	27

ABSTRACT

The iridium alloy DOP-26 is used to produce Clad Vent Set cups that protect the radioactive fuel in radioisotope thermoelectric generators (RTGs) which provide electric power for spacecraft and rovers. In a previous study, the tensile properties of DOP-26 were measured over a wide range of strain rates and temperatures and reported in ORNL/TM-2007/81. While that study established the properties of the base material, the fabrication of the heat sources requires welding, and the mechanical properties of welded DOP-26 have not been extensively characterized in the past. Therefore, this study was undertaken to determine the mechanical properties of DOP-26 specimens containing a transverse weld in the center of their gage sections. Tensile tests were performed at room temperature, 750, 900, and 1090°C and engineering strain rates of 1×10^{-3} and 10 s^{-1} . Room temperature testing was performed in air, while testing at elevated temperatures was performed in a vacuum better than 1×10^{-4} Torr. The welded specimens had a significantly higher yield stress, by up to a factor of ~ 2 , than the non-welded base material. The yield stress did not depend on the strain rate except at 1090°C, where it was slightly higher for the faster strain rate. The ultimate tensile stress, on the other hand, was significantly higher for the faster strain rate at temperatures of 750°C and above. At 750°C and above, the specimens deformed at $1 \times 10^{-3} \text{ s}^{-1}$ showed pronounced necking resulting sometimes in perfect chisel-edge fracture. The specimens deformed at 10 s^{-1} exhibited this fracture behavior only at the highest test temperature, 1090°C. Fracture occurred usually in the fusion zone of the weld and was, in most cases, primarily intergranular.

1. INTRODUCTION

Iridium exhibits a unique combination of a high melting point (2443°C), good oxidation resistance, and excellent high-temperature strength [1]. In a review of 25 years of research on iridium as a structural material, George and Liu [1] reported that its mechanical properties can be significantly improved by macroalloying (typically $>1 \text{ wt}\%$) and microalloying (typically $<1 \text{ wt}\%$). Macroalloying with W or Hf increases the yield strength and the recrystallization temperature [1-6]. Microalloying with Th impedes grain growth and increases the tensile impact ductility by strengthening the grain boundaries [1-5]. The beneficial effect of Th is due to its segregation at the grain boundaries [7] and the formation of fine Ir_5Th precipitates [8]. The Th may be partially substituted with Ce without any loss in the mechanical properties [9,10]. In fact, alloys containing Th plus Ce with improved high-temperature impact ductility and weldability have been developed at Oak Ridge National Laboratory (ORNL) [1].

An important use of iridium is in radioisotope thermoelectric generators (RTGs) for space power applications [11]. In RTGs, the iridium alloy DOP-26 that was developed at ORNL [1-5] is used as cladding for $^{238}\text{PuO}_2$ fuel. DOP-26 is an Ir-0.3 wt% W alloy containing 60 wppm Th to improve the high temperature impact ductility. Iridium as well as DOP-26 exhibit the face-centered cubic crystal structure. Unlike other metals with this crystal structure, their mechanical properties are strain rate sensitive. The mechanical behavior of iridium thus resembles that of body-centered cubic metals [1]. As a result of the strain rate sensitivity, the ductility of iridium decreases with increasing strain rate, especially at impact strain rates, e.g., $\sim 10^3 \text{ s}^{-1}$ [10]. These observations provided the motivation for a previous study [12] in which the mechanical properties of DOP-26 at temperatures from room temperature to 1090°C and strain rates from 10^{-3} to 50 s^{-1} were investigated.

The fabrication of Clad Vent Set cups for RTGs involves gas tungsten arc welding (GTAW) of DOP-26. Liu and David [13,14] have examined the weld metal grain structure and tensile mechanical properties of welded DOP-26 at one temperature (650°C) and one strain rate ($3.3 \times 10^{-3} \text{ s}^{-1}$). The present work adds to that information by examining the mechanical properties of welded DOP-26 over a wide

range of temperatures and strain rates. The results presented will help to model the mechanical behavior of welded Clad Vent Sets more precisely.

2. EXPERIMENTAL PROCEDURE

2.1. WELDING

DOP-26 blanks with a diameter of 52 mm were fabricated, using electrical discharge machining (EDM), from hot-rolled and ground sheet with a thickness ranging from 0.63 to 0.68 mm. The blanks were processed according to Test Plan ORNL-WTT-TP4, Rev. 1. Blank/specimen processing was documented using WELDED IRIIDIUM ALLOY TENSILE TEST SPECIMEN PREPARATION TRAVELER (Appendix A). First, the blanks were acid cleaned and recrystallized for 1 h at 1375°C in vacuum. Then, full penetration bead-on-plate welds using GTAW in an inert atmosphere glovebox were made to produce welds meeting the dimensional and grain size requirements of the Fueled Clad welds made at Los Alamos National Laboratory (LANL). Welding was conducted along the diameter of each blank parallel to the rolling direction (Fig. 1). The glovebox atmosphere consisted of argon with less than 1 ppm (parts per million) oxygen and approximately 20 ppm moisture. To maintain flatness of the welded blanks and to provide constant heat sinking, the blanks were rigidly clamped in a Sigmajig welding fixture [15]. This fixture includes a stationary clamp that can be attached to one side of the DOP-26 blank and a moveable clamp that can be attached to the other side, thereby allowing tension to be applied transverse to the welding direction. A stress of approximately 27.5 MPa, which is significantly below the threshold stress to develop hot cracking during welding, was applied prior to welding.

Welding parameters were developed at ORNL that produce full penetration welds with a grain structure equivalent to that of welded Fueled Clads produced at LANL. The welding process included four pole magnetic oscillation that is used to suppress hot cracking in DOP-26. During welding, the welding current was continuously decreased to compensate for heat buildup and maintain a constant fusion zone width of ~2.5 mm. The welding parameters are shown in Table 1. These parameters resulted in welds with relatively flat weld faces and weld roots, and thicknesses that were approximately 50 μm greater than those of the blank.

Table 1. Welding Parameters

Welding Current	93 A decreasing to 92 A
Welding Speed	12.7 mm/s (30 inches per minute)
Arc Length	0.9 mm (.035 inch)
Glovebox Atmosphere	Argon
Torch Shield Gas	75% Helium-25% Argon
4 Pole Magnetic Oscillation	On
X Axis Amplitude	94%
Y Axis Amplitude	8%
Frequency	55 Hz

2.2. SPECIMEN FABRICATION

After welding, tensile specimens were fabricated, using EDM, from the recrystallized DOP-26 iridium blanks followed by grinding of their gage and fillet radii sections to the final dimensions (Fig. 1). The specimens were cut such that their long (tensile) axes were perpendicular to the weld line. This means that they were oriented transverse to the rolling direction, and that the weld was transverse with respect to the specimen. The ground faces of the gage sections and fillet radii as well as the remaining EDM specimen faces were polished with 320-grit and 600-grit SiC papers. After dimensional inspection, the specimens were cleaned per procedure GPHS-Y-005. This entailed using an ultrasonic detergent bath heated to 65°C for 10 minutes followed by rinsing in demineralized water then immersing for 15 minutes in each of three acid baths heated to 70°C: a) 3 parts HF:7 parts HNO₃, b) 3 parts HCl:1 part HNO₃, and c) 1 part HNO₃. Demineralized water rinsing was done between baths followed by final rinsing in demineralized water. Of the 32 specimens tested, all but 6 were given an additional “Module Reduction Monitoring (MRM) heat treatment” (1140°C/1176 h/vacuum). The gage length of each specimen was then marked with a row of ten 1000-g-load microhardness impressions spaced at 0.9-mm intervals.

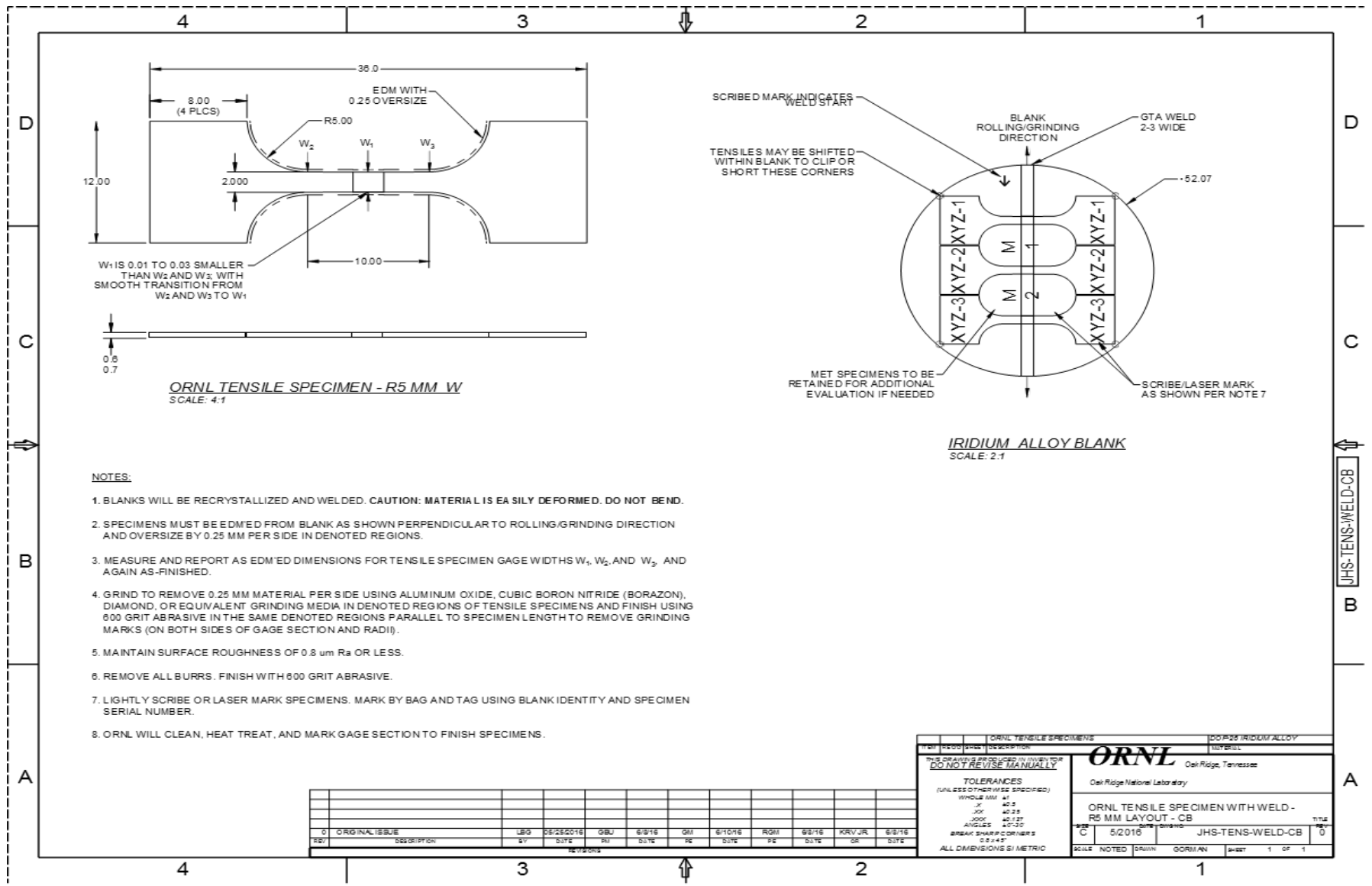


Fig. 1. Drawing of tensile test specimen with machining instructions.

2.3. MECHANICAL TESTING

Tensile tests were carried out in a servohydraulic 1321 Instron testing machine. The test matrix in Table 2 indicates the heat treat conditions, test temperatures and strain rates used. The tensile specimens were tested and data was recorded in accordance with Standard Operating Procedure MET-ABAD-SOP-25.

Table 2. Test Matrix for Tensile Specimens showing the Number of Tests carried out for each Heat Treat Condition/Test Temperature/Strain Rate Combination.

Strain Rate s^{-1} Test Temp. $^{\circ}C$	10^{-3}	10
RT	3	3
750	3	3
750 (no MRM)	3	---
900	3	3
1090	5	3
1090 (no MRM)	3	---

The Instron is equipped with a turbo-pumped vacuum system and a radio frequency (RF) heater to inductively heat a tantalum susceptor supported by an alumina tube. The specimens are placed inside this assembly and heated by radiation from the susceptor. This system is the same as that used in the earlier study of non-welded DOP-26 [12]. Prior to testing, each specimen was inserted into mating molybdenum alloy (TZM) grips supporting it on its 5 mm radius shoulders. Room temperature tests were performed in air. Tests above room temperature were performed in a vacuum better than 1×10^{-4} Torr. The specimen temperature was measured with two Pt-Pt/Rh type S thermocouples that were placed on the specimen gage section and wrapped with 0.4 mm diameter Pt wire. The distance between the two thermocouples was typically 5 mm. During testing, the temperature was held within $\pm 10^{\circ}C$ of the target value. The load cell was calibrated with an accuracy of $\pm 1\%$ of its reading. The thickness of each specimen was measured with a point micrometer in five places along its gage and the smallest of these readings was chosen as the thickness for the calculation of the stress. The initial cross-sectional area of the specimens was determined from the specimen thickness and width W_1 (Fig. 1) measured with an accuracy of 1%, resulting in an overall accuracy of the stress calculation of $\pm 2\%$.

The low yield stress and small size of the specimens precluded the attachment of an extensometer to the gage length for measuring strain. Instead, strain was determined from the crosshead displacement, which was calculated from the crosshead velocity and time. The load cell signal exhibited some noise, in particular when the induction unit was running. For the strain rate of $10^{-3} s^{-1}$ the resulting stress signal was therefore smoothed. At the higher strain rate of $10 s^{-1}$ data points were collected only every 0.2% of strain and the number of data points collected was considered insufficient to allow smoothing.

For the evaluation of the tensile test data, uncorrected specimen strains, i.e., “*crosshead strains*,” were obtained by dividing the crosshead displacement by the nominal gage length, 10 mm. Plots of stress versus crosshead strain, such as that shown in Fig. 2, were then constructed. An *elastic line* was drawn through the linear slope region of the stress-strain curve (the region prior to reaching the yield point), and an *elastic line at fracture* with the same slope was drawn through the point of fracture as shown in Fig. 2. In the case of sudden fracture at or after reaching the ultimate tensile stress (UTS), the elastic line at fracture was placed through that point. In the case of gradual fracture, the elastic line was placed through a point on the descending part of the stress-strain curve at 0.8 times the UTS. The “*crosshead*

fracture strain” was defined as the horizontal separation between the elastic line and the elastic line at fracture. The “*crosshead plastic strain*” for each point on the test curve in Fig. 2 was defined as the horizontal distance between the elastic line and that point.

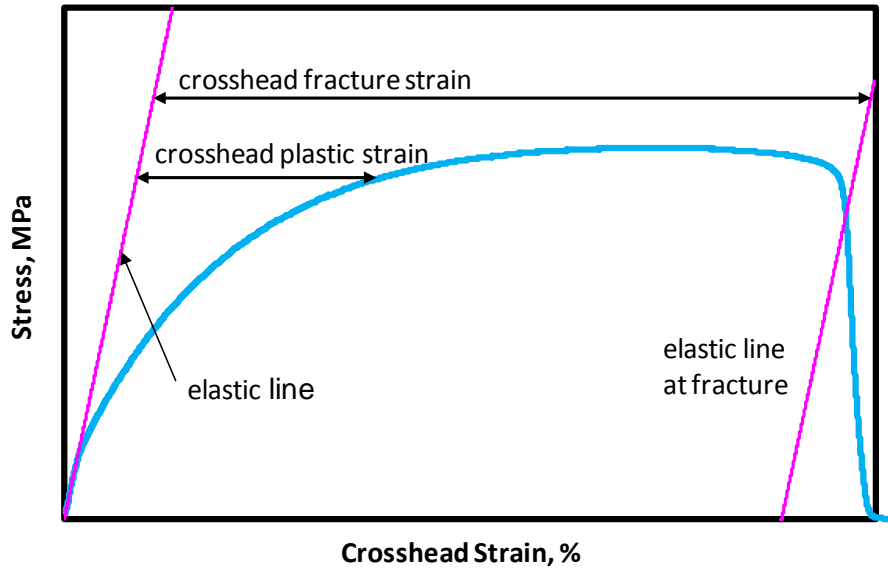


Fig. 2. Schematic of stress vs. crosshead strain.

Deformation of the specimens did not occur exclusively in the 10-mm gage length. During testing, plastic seating effects occurred in the shoulders of the specimens, and due to work hardening plastic deformation propagated from the gage sections into the shoulder regions. The seating effects in the specimen shoulders result in the “elastic line” being not truly elastic, but for convenience this term will be used. Because plastic deformation is not restricted to the gage length, the crosshead fracture strain overestimates the actual plastic strains incurred in the gage. In order to obtain a more accurate measure of the specimen plastic strain, corrections using the “*indent fracture strain*” were made as described below.

The indent fracture strain was calculated from the average increase of the spacings between the microhardness indents after fracture. For each specimen, the crosshead fracture strain was multiplied by a *strain correction factor* chosen such that the observed indent fracture strain was obtained. The “*corrected crosshead plastic strain*” for each specimen was then calculated by multiplying the crosshead plastic strain with this strain correction factor. The “*corrected crosshead fracture strain*” is the corrected crosshead plastic strain at fracture. It is identical to the indent fracture strain. The final plots of (engineering) stress vs. (engineering) strain were obtained from curves of the stress vs. the crosshead strain by replacing the crosshead plastic strain with the corrected crosshead plastic strain. The **corrected strain** used in the curves shown hereafter is the sum of the elastic strain (calculated from the elastic line) and the corrected crosshead plastic strain. The 0.2% offset yield stresses were calculated by shifting the elastic line by a corrected crosshead plastic strain of 0.2% to the right and determining its intersection with the stress-strain curve.

3. RESULTS AND DISCUSSION

3.1 MICROSTRUCTURE OF WELDS

Typical microstructures on planes parallel and perpendicular to the welded blanks are shown in Figs. 3 and 4, respectively. The welds consist of large elongated grains originating at, and growing epitaxially from, the fusion line towards the center line of the weld. At the center of the weld, grain growth competition and changes in growth direction produce small grains. In DOP-26 weldments the heat affected zone (HAZ) is difficult to detect, and probably quite narrow, since grain growth is severely restricted due to grain boundary pinning by the Ir_5Th precipitates. In other words, the weld region consisting of the fusion zone and the HAZ on either side is more or less the same as the fusion zone.

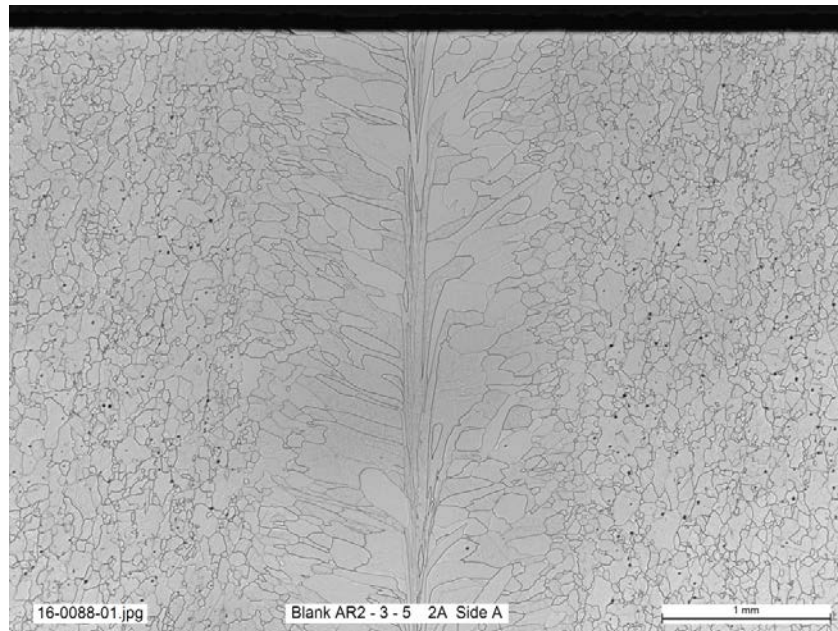


Fig. 3. Light microscope image showing the microstructure of the weld region and base metal in a plane parallel to the plane of the blank. During welding, the weld bead progressed from the top to the bottom of the micrograph.

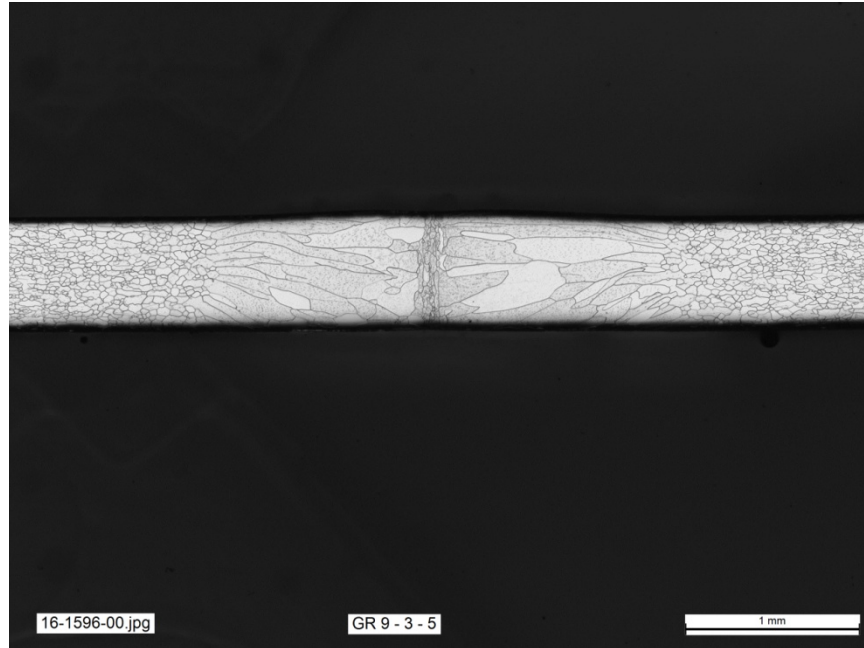


Fig. 4. Light microscope image showing the microstructure of the weld region and base metal in a plane perpendicular to the plane of the blank.

To confirm that the weld grain structure was equivalent to that of fueled clads, specimens for metallurgical evaluation were removed from three blanks representing the first, last, and middle of the weld campaign. These welds were evaluated according to the same criteria used for production example welds (see LANL procedure RPS-TA55-302, “Examination of Example Welds”). All weld sections met the LANL weld criteria. Typical results of the metallurgical evaluation are summarized in Table 3.

Table 3. Results of Metallurgical Evaluation of Welds

Blank Identity: GR9-3-5						
Number of Grains Through Thickness at a given Distance from Weld Centerline (C/L) (mm)						
-2	-1.2	-0.6	C/L (0)	0.6	1.2	2.0
23	18	12	23	8	16	23
Any weld grain > 50% of weld thickness: No						
Minimum of 6 grains through the weld at specified locations: Yes						
Cracks, porosity or other observable defects: No						

3.2. STRESS-STRAIN CURVES

Figures 5-14 depict the stress-strain curves evaluated as described earlier. As pointed out before, the corrected strain in these curves is the sum of the strains given by the elastic line and the corrected plastic crosshead strain.

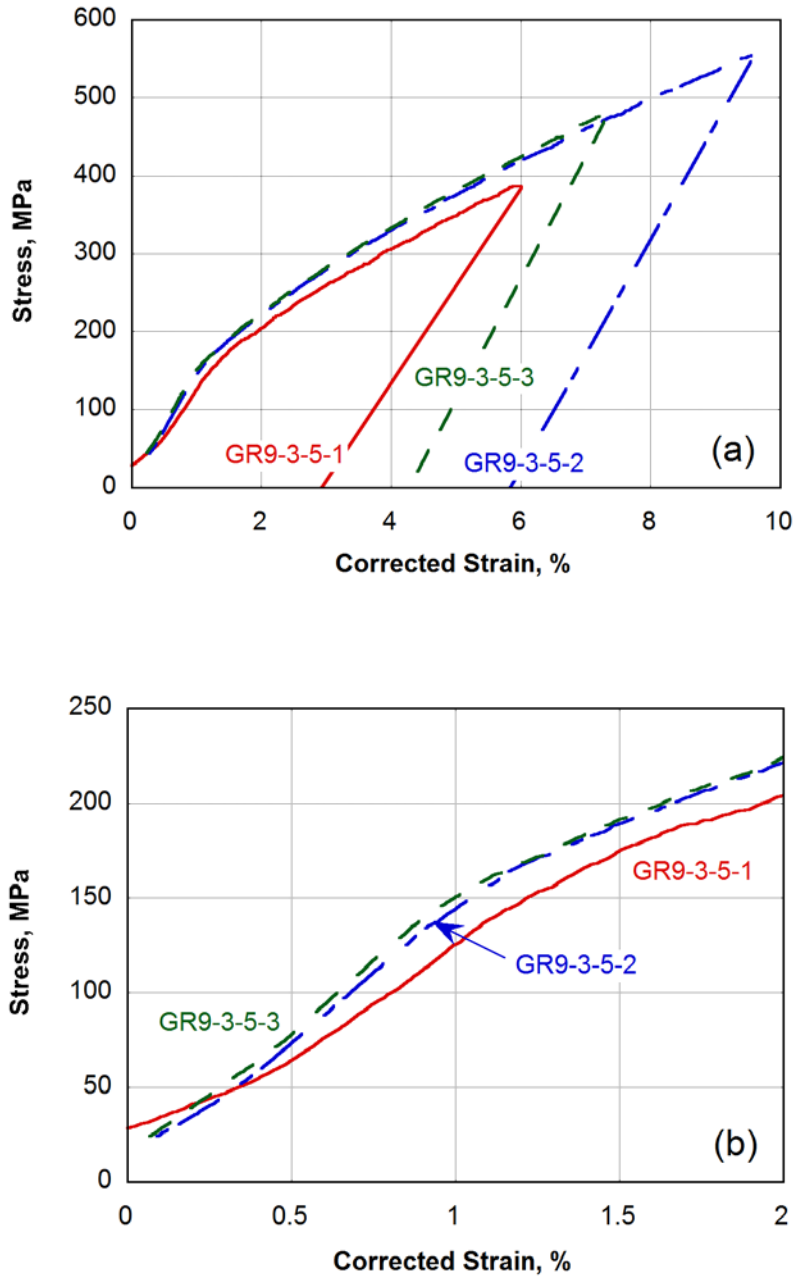


Fig. 5. Stress-strain curves for welded DOP-26 with MRM heat treatment tested at 10^{-3} s^{-1} and 25°C , (a) full curves, (b) yield region.

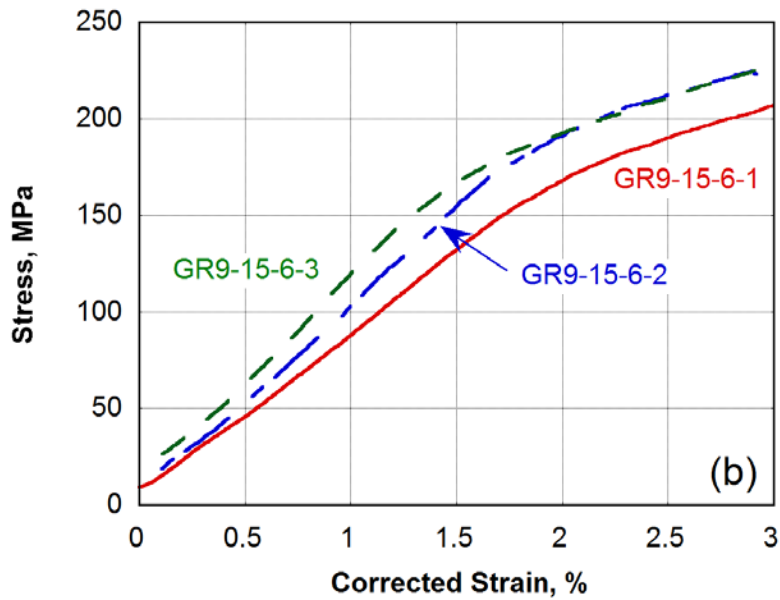
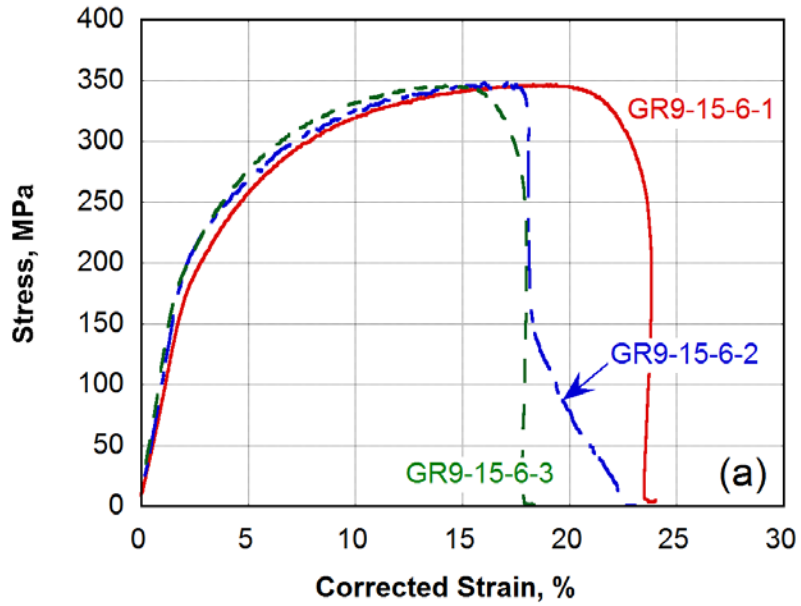


Fig. 6. Stress-strain curves for welded DOP-26 without MRM heat treatment tested at 10^{-3} s^{-1} and 750°C , (a) full curves, (b) yield region.

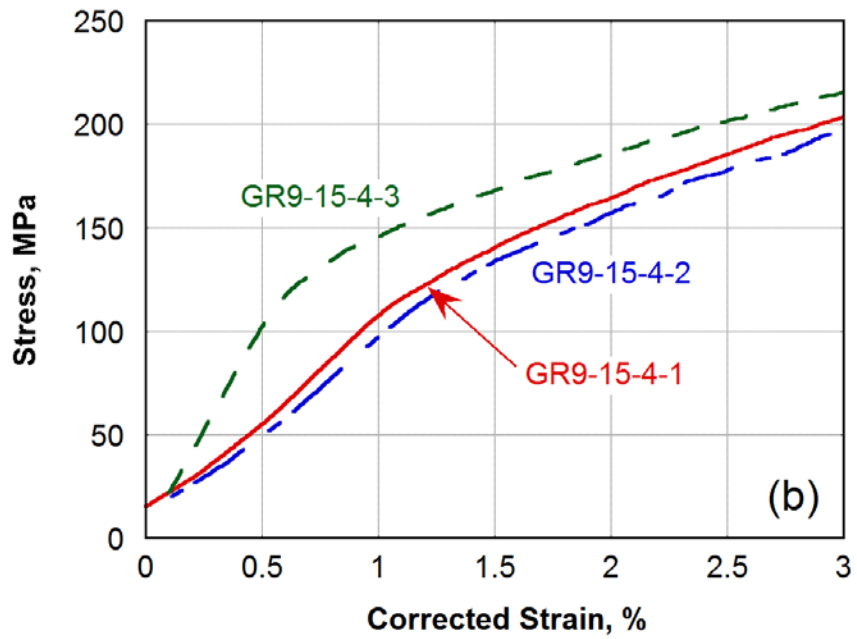
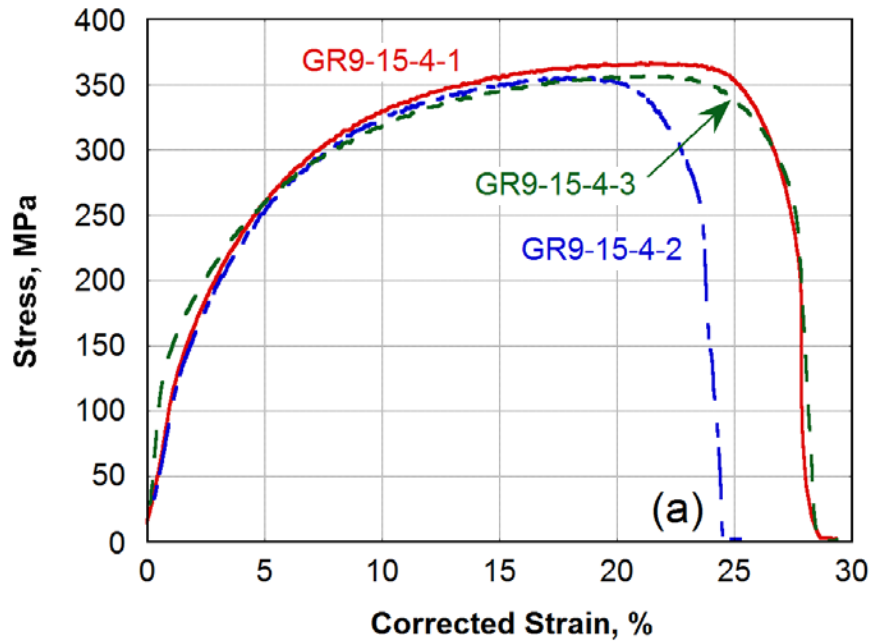


Fig. 7. Stress-strain curves for welded DOP-26 with MRM heat treatment tested at 10^{-3} s^{-1} and 750°C , (a) full curves, (b) yield region.

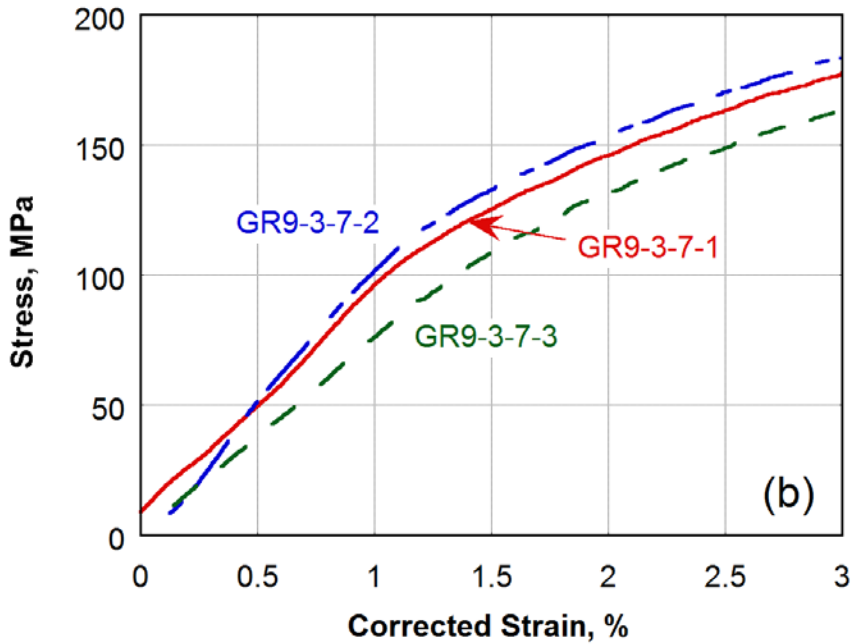
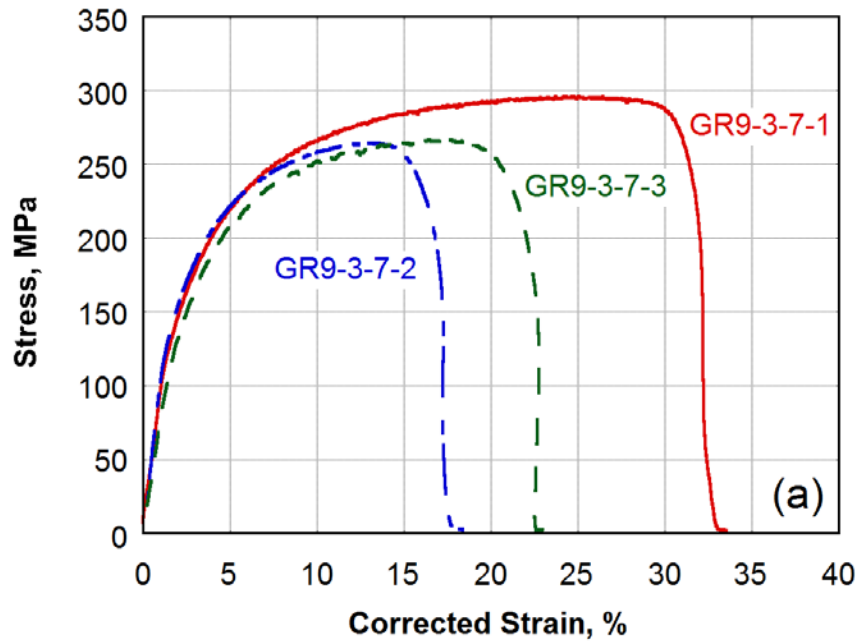


Fig. 8. Stress-strain curves for welded DOP-26 with MRM heat treatment tested at 10^{-3} s^{-1} and 900°C , (a) full curves, (b) yield region.

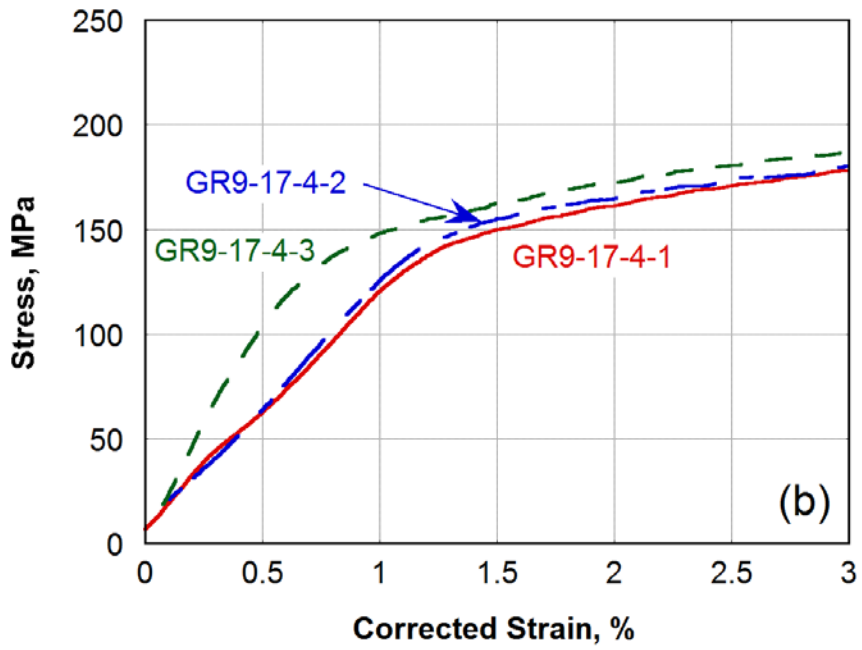
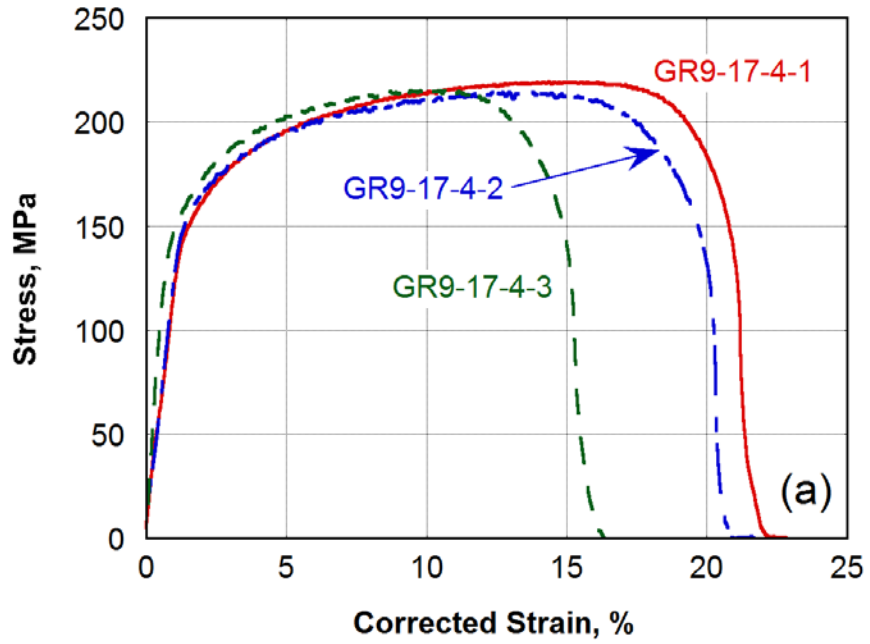


Fig. 9. Stress-strain curves for welded DOP-26 without MRM heat treatment tested at 10^{-3} s^{-1} and 1090°C , (a) full curves, (b) yield region.

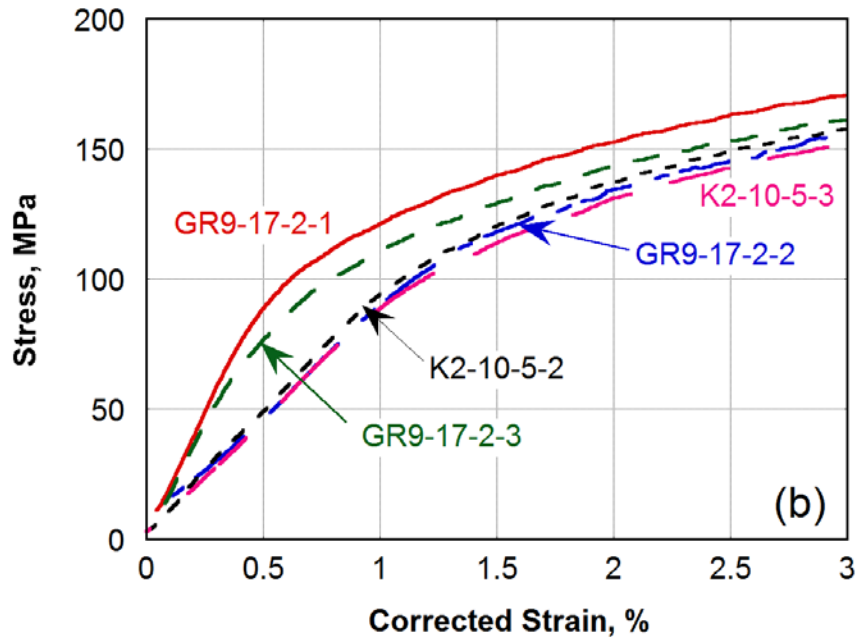
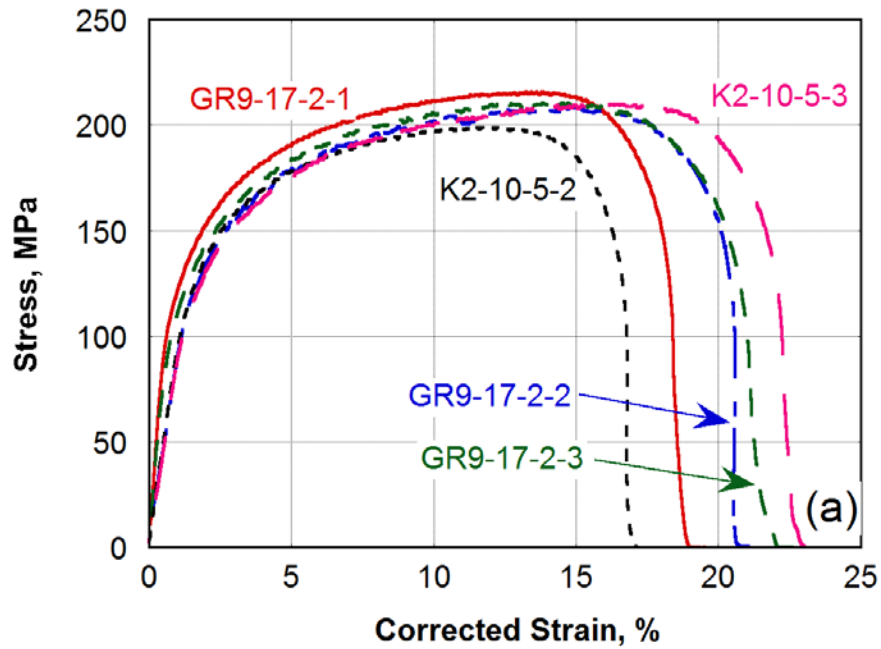


Fig. 10. Stress-strain curves for welded DOP-26 with MRM heat treatment tested at 10^{-3} s^{-1} and 1090°C , (a) full curves, (b) yield region.

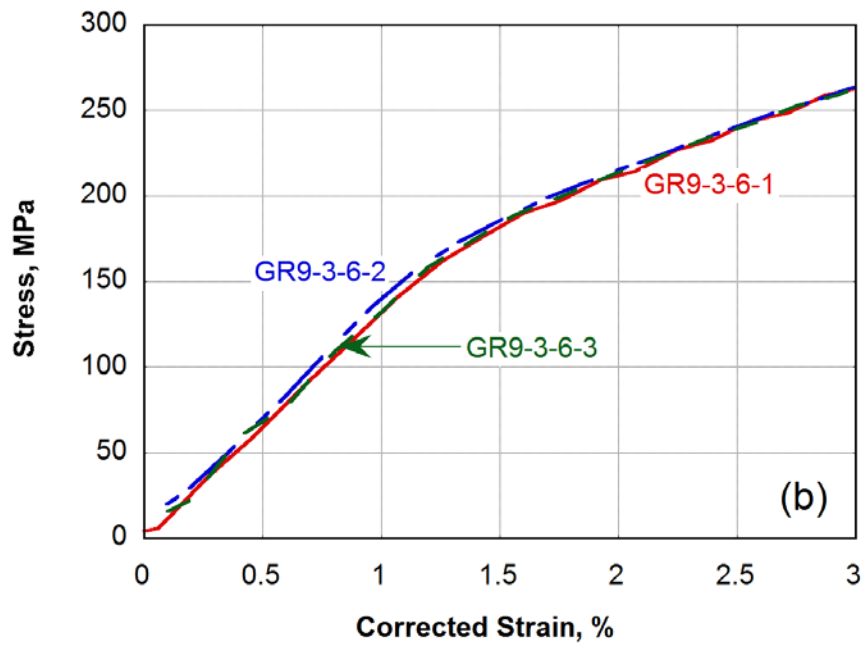
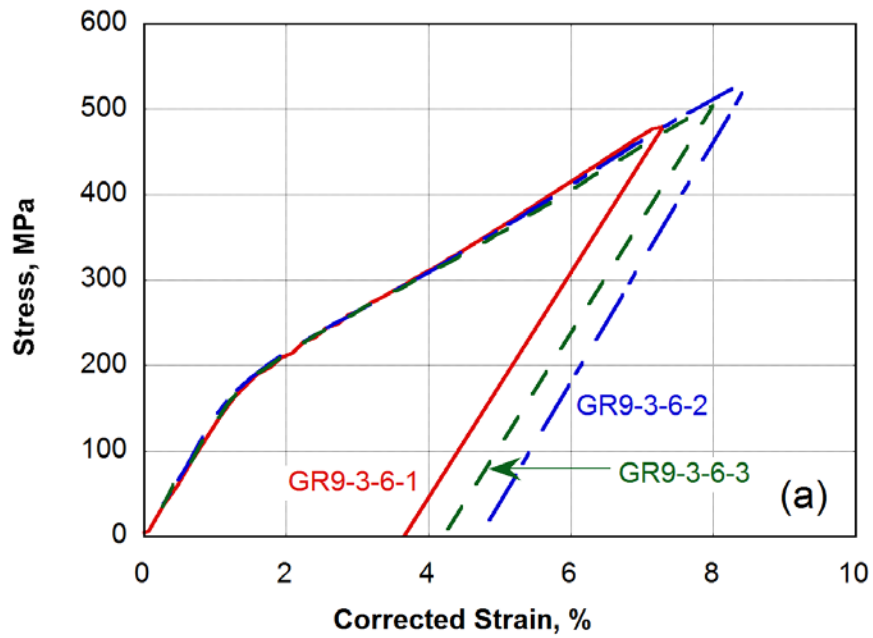


Fig. 11. Stress-strain curves for welded DOP-26 with MRM heat treatment tested at 10 s^{-1} and 25°C , (a) full curves, (b) yield region.

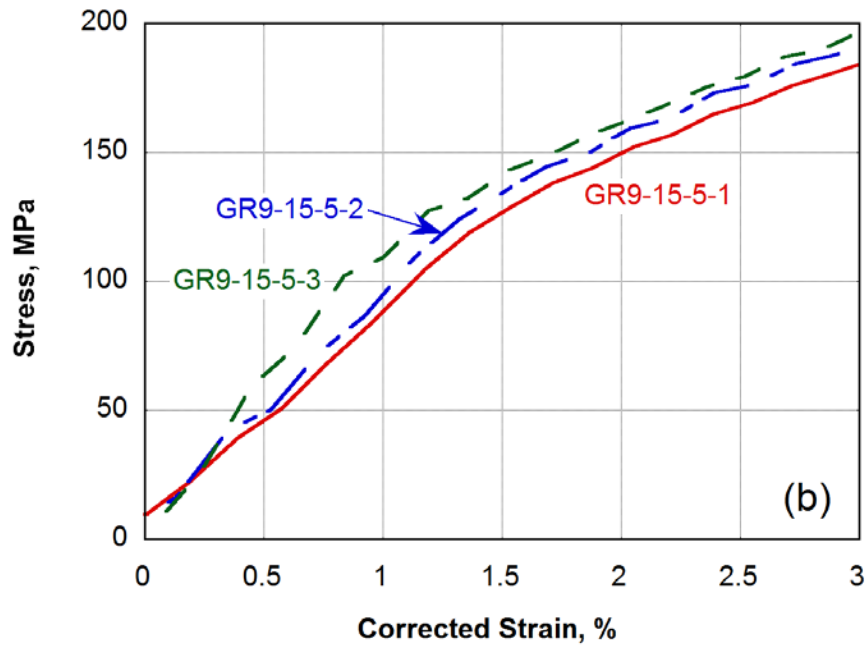
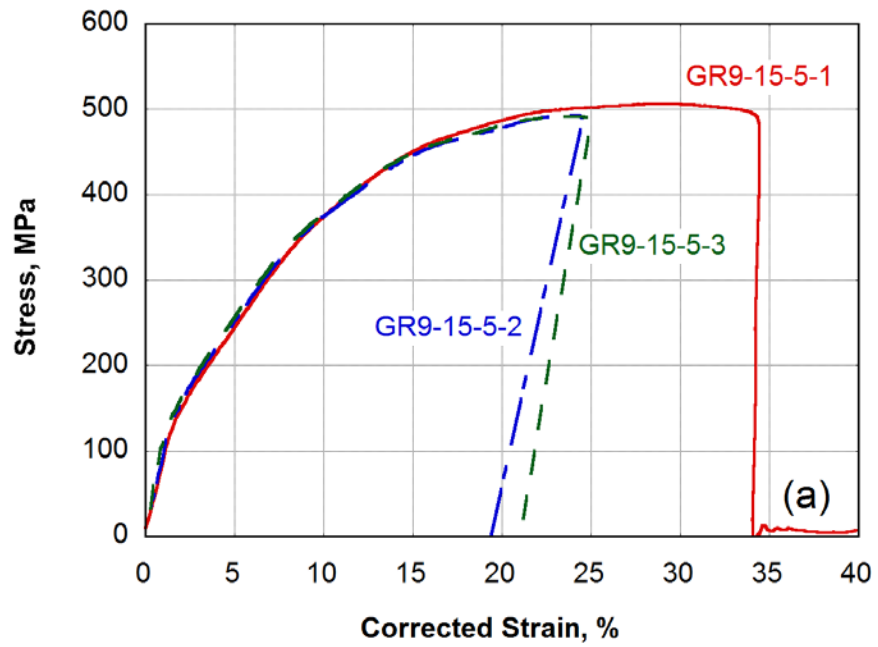


Fig. 12. Stress-strain curves for welded DOP-26 with MRM heat treatment tested at 10 s^{-1} and 750°C , (a) full curves, (b) yield region.

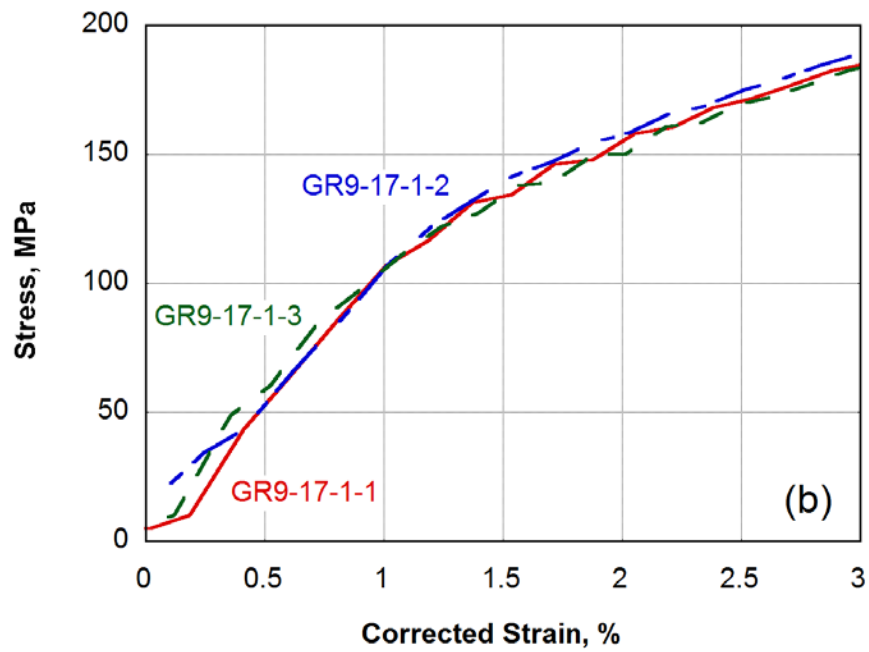
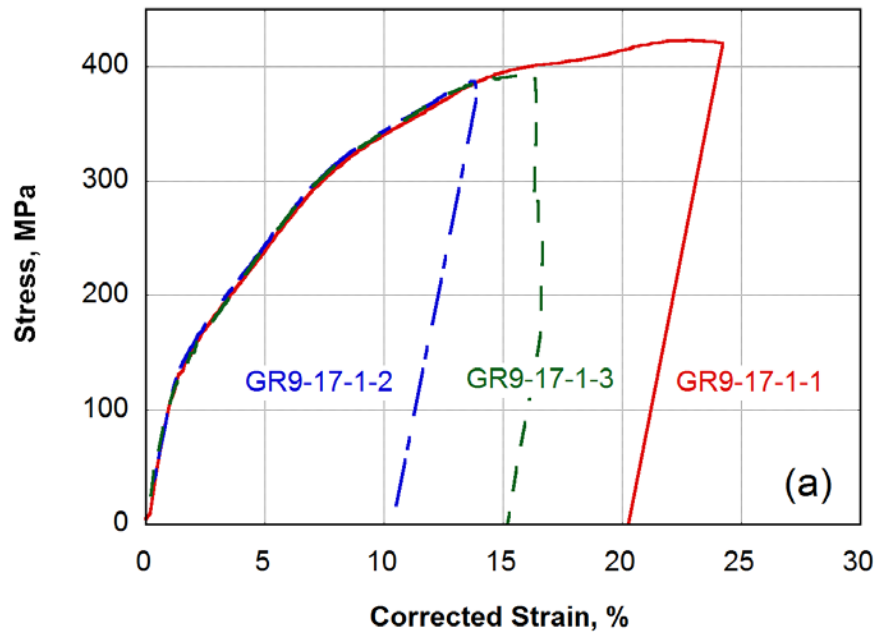


Fig. 13. Stress-strain curves for welded DOP-26 with MRM heat treatment tested at 10 s^{-1} and 900°C , (a) full curves, (b) yield region.

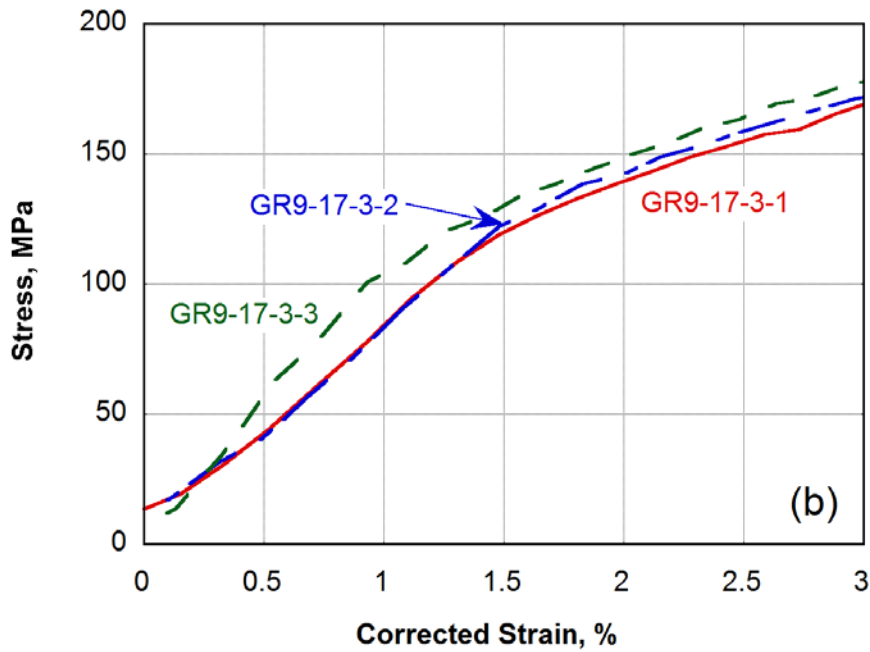
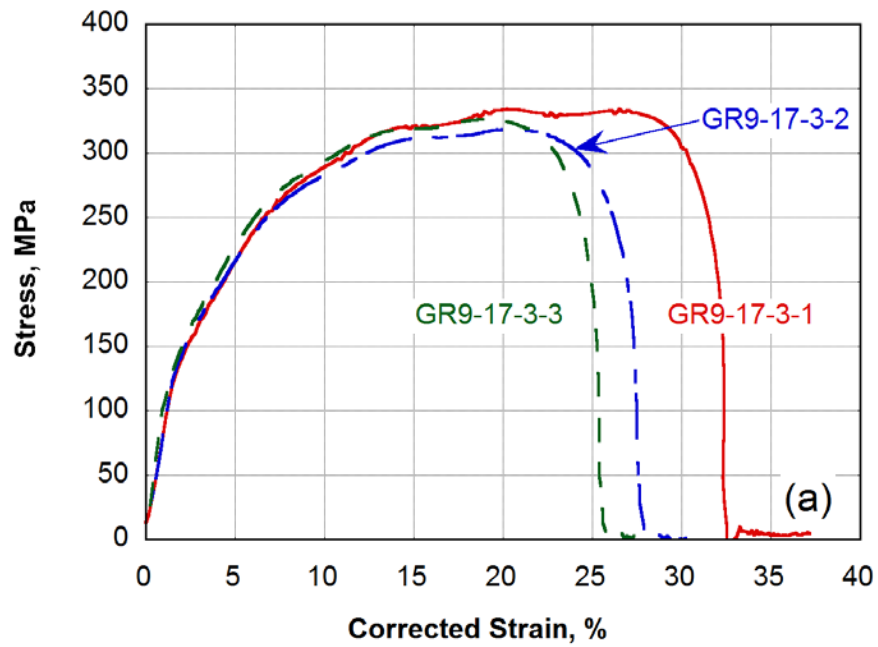


Fig. 14. Stress-strain curves for welded DOP-26 with MRM heat treatment tested at 10 s^{-1} and 1090°C , (a) full curves, (b) yield region.

3.3. EVALUATION AND DISCUSSION OF STRESS-STRAIN CURVES

Tables 4 and 5 summarize the parameters and mechanical properties obtained from the evaluation of the stress-strain curves in Figs. 5-14. For each temperature and strain rate combination three specimens were tested (except at 1090°C and $1 \times 10^{-3} \text{ s}^{-1}$, where five nominally identical specimens were tested to check the reproducibility of the data). In Table 5 it should be noted that the data for the DOP-26 base material adopted from the 2007 report [12] were for specimens longitudinally oriented with respect to the rolling direction, whereas the present results are for the transverse direction. However, since there is no significant difference in the properties of these two directions [12] the comparisons made are valid. Figures 15-18 present the results in graphical form using average values and error bars. In some cases, the temperatures were shifted slightly to prevent overlap of the error bars. The lines in these figures are only meant as a guide for the eye.

It needs to be pointed out that Figs. 15-18 compare welded material **with** MRM heat treatment to base material **without** that heat treatment. As will be evident from an inspection of the data, the differences between the yield stresses and fracture strains of the welded vs. the base material would be even larger if the welded material had not been given the MRM heat treatment. Several important observations can be made:

- (a) As evidenced by the tests carried out at $1 \times 10^{-3} \text{ s}^{-1}$ and 750 and 1090°C, the MRM heat treatment reduces the yield stress of welded DOP-26 significantly (see Table 5).
- (b) The welded specimens have a higher yield stress than the non-welded base material examined in the 2007 report [12]. This increase can be substantial: for example, at $1 \times 10^{-3} \text{ s}^{-1}$ and 750°C the average yield stress of the welded material without MRM heat treatment is 186 MPa, whereas the non-welded base material exhibits an average yield stress of 80 MPa.
- (c) At room temperature, the UTS of the welded material is significantly lower than the UTS of the base material. However, at 750°C and above, the UTS of the welded specimens is about the same as for the base material.
- (d) The yield stress of the welded specimens is not significantly affected by the strain rate except at 1090°C, where it is somewhat higher for the faster strain rate (10 s^{-1}). The room temperature UTS is not significantly affected by the strain rate, but at 750°C and above the higher strain rate results in significantly higher UTS values. This result is qualitatively similar to that obtained in the 2007 report (see Fig. 25 in [12]).
- (e) The fracture strain of welded DOP-26 is generally lower than that of the base material. This difference is largest at room temperature where the base material exhibits a fracture strain of ~10%, whereas the welded material fractures at ~4%. At 750°C and above the welding decreases the fracture strain from ~35% to ~20%. The significantly lower room-temperature ductility is one reason for the correspondingly lower room-temperature UTS (since the material has less opportunity to work harden).
- (f) Of the thirty-two specimens examined, three fractured outside the fusion zone of the weld (see Tables 4 and 5). For each temperature and strain rate combination, the specimens that fractured outside the fusion zone exhibited a larger fracture strain than those that fractured within the fusion zone. This is consistent with the larger fracture strains of the base material.

Observation (b) in the list above deserves additional discussion. Liu and David [13,14] examined DOP-26 with and without a transverse weld. Their heat treatment before welding consisted of 1 h at 1500°C, and the welded specimen was not subjected to an MRM heat treatment. They found that welding increased the yield stress at 650°C from 85.4 to 173.6 MPa. Our results in Table 5 for the specimen tested at $1 \times 10^{-3} \text{ s}^{-1}$ and 750°C (without MRM heat treatment) are consistent with Liu and David's findings. However, it must be noted that the experimental conditions of the two studies are not the same: Liu and David used a test temperature of 650 vs. 750°C (here), and a heat treatment of 1500°C/1 h vs. 1375°C/1 h (here). The lower test temperature of Liu and David would be expected to increase the yield stress while the higher heat treatment temperature, by increasing the grain size, would be expected to decrease the yield stress. It may be fortuitous that these two opposing tendencies produced yield stress values that are very similar in the two studies. Regardless of the exact magnitudes, though, both studies show an increase of yield stress after welding.

The precise reasons for the increase in the yield stress due to welding are not known at the present time, and several factors may be involved. As the liquid in the weld pool solidifies and cools down to room temperature, substantial shrinkage occurs. With densities of 19.5 and 20.9 Mg/m³ for liquid and solid iridium at the melting point [16,17] the volume shrinkage during solidification is found to be ~7%, corresponding to a linear contraction of ~2.3%. Cooling of solid Ir from its melting point to room temperature causes a linear contraction of ~2.6% [17]. During cool down it is therefore expected that internal stresses build up in the fusion zone and the adjacent base material. It is conceivable that these stresses cause internal plastic deformation. Since the work hardening of iridium is very pronounced, relatively small strains would be sufficient to increase its strength: at room temperature a plastic strain of 1% would strengthen the material by ~100 MPa, which is similar to the yield stress increase we find in welded DOP-26. However, this "internal deformation" argument would require that the material on either side of the fusion zone deforms sufficiently to cause the observed yield stress increase. In the case of the present specimens, sufficient deformation would have to have occurred in a region at least 4 mm away from either side of the fusion zone. There are other factors which may be important as well. For example, the grains in the fusion region are likely to be textured and this may increase the yield stress and strengthen, due to constraint effects, the adjacent base material. This argument again depends critically on how far away from the fusion zone such a constraint effect would operate. Further work would be required to answer these questions.

Table 4. Fracture Strains and Slopes of Elastic Lines for Welded DOP-26

ID	MRM Heat Treatment	Strain Rate, s ⁻¹	Temp., °C	Indent Fracture Strain, % ⁺⁺	Crosshead Fracture Strain, %	Ratio of Indent and Crosshead Fracture Strains	Slope of Elastic Line, MPa/(% Crosshead Strain)
GR9-3-5-1*	Yes	1×10 ⁻³	25	2.9	3.0	0.97	125
GR9-3-5-2	Yes	1×10 ⁻³	25	5.8	6.6	0.88	147
GR9-3-5-3	Yes	1×10 ⁻³	25	4.3	5.2	0.83	156
GR9-15-6-1	No	1×10 ⁻³	750	20.2	33.5	0.60	91
GR9-15-6-2	No	1×10 ⁻³	750	15.4	22.4	0.69	105
GR9-15-6-3	No	1×10 ⁻³	750	15.5	28.1	0.55	122
GR9-15-4-1	Yes	1×10 ⁻³	750	24.1	33.8	0.71	108
GR9-15-4-2	Yes	1×10 ⁻³	750	20.1	27.3	0.74	97
GR9-15-4-3	Yes	1×10 ⁻³	750	25.7	36.6	0.70	214
GR9-3-7-1 ⁺	Yes	1×10 ⁻³	900	29.2	44.4	0.66	94
GR9-3-7-2	Yes	1×10 ⁻³	900	14.6	26.7	0.55	103
GR9-3-7-3	Yes	1×10 ⁻³	900	19.0	31.5	0.60	76
GR9-17-4-1	No	1×10 ⁻³	1090	18.8	32.7	0.57	121
GR9-17-4-2	No	1×10 ⁻³	1090	17.6	28.9	0.61	127
GR9-17-4-3	No	1×10 ⁻³	1090	13.6	25.6	0.53	232
GR9-17-2-1	Yes	1×10 ⁻³	1090	16.6	29.7	0.56	195
GR9-17-2-2	Yes	1×10 ⁻³	1090	17.8	30.5	0.58	92
GR9-17-2-3	Yes	1×10 ⁻³	1090	18.4	28.0	0.66	177
K2-10-5-2	Yes	1×10 ⁻³	1090	14.4	28.3	0.51	97
K2-10-5-3	Yes	1×10 ⁻³	1090	19.3	31.2	0.62	91
GR9-3-6-1	Yes	10	25	3.7	5.3	0.70	132
GR9-3-6-2	Yes	10	25	4.7	6.4	0.73	141
GR9-3-6-3	Yes	10	25	4.2	5.4	0.78	133
GR9-15-5-1 ⁺	Yes	10	750	29.9	40.1	0.75	89
GR9-15-5-2	Yes	10	750	19.4	24.0	0.81	96
GR9-15-5-3	Yes	10	750	21.1	27.5	0.77	122
GR9-17-1-1	Yes	10	900	20.3	26.1	0.78	106
GR9-17-1-2	Yes	10	900	10.4	14.1	0.74	106
GR9-17-1-3	Yes	10	900	13.7	19.4	0.71	119
GR9-17-3-1 ⁺	Yes	10	1090	28.0	40.9	0.68	84
GR9-17-3-2*	Yes	10	1090	23.0	31.1	0.74	83
GR9-17-3-3*	Yes	10	1090	21.7	31.7	0.68	109

*Specimen slightly curved after MRM heat treatment

⁺Fracture outside of fusion zone

⁺⁺Identical to the “corrected crosshead fracture strain”

Table 5. Fracture Strains, Yield Stresses and Ultimate Tensile Stresses for Welded DOP-26 (Present Study) and DOP-26 Base Material (ORNL/TM-2007/81, Ref [12])

ID	Weld	MRM Heat Treatment	Strain Rate, s ⁻¹	Temp., °C	Indent Fracture Strain, % ⁺⁺	0.2% Offset Yield Stress, MPa	Ultimate Tensile Stress, MPa
#1, #32, #43 [12]	No	No	1×10 ⁻³	25	9.2	124	720
GR9-3-5-1*	Yes	Yes	1×10 ⁻³	25	2.9	189	387
GR9-3-5-2	Yes	Yes	1×10 ⁻³	25	5.8	187	556
GR9-3-5-3	Yes	Yes	1×10 ⁻³	25	4.3	181	482
#20, #35 [12]	No	No	1×10 ⁻³	750	31.6	80	342
GR9-15-6-1	Yes	No	1×10 ⁻³	750	20.2	181	346
GR9-15-6-2	Yes	No	1×10 ⁻³	750	15.4	199	347
GR9-15-6-3	Yes	No	1×10 ⁻³	750	15.5	178	345
GR9-15-4-1	Yes	Yes	1×10 ⁻³	750	24.1	139	367
GR9-15-4-2	Yes	Yes	1×10 ⁻³	750	20.1	141	355
GR9-15-4-3	Yes	Yes	1×10 ⁻³	750	25.7	140	356
#4, #21, #36 [12]	No	No	1×10 ⁻³	900	35.7	80	282
GR9-3-7-1 ⁺	Yes	Yes	1×10 ⁻³	900	29.2	125	295
GR9-3-7-2	Yes	Yes	1×10 ⁻³	900	14.6	131	264
GR9-3-7-3	Yes	Yes	1×10 ⁻³	900	19.0	128	266
#5, #37, #45 [12]	No	No	1×10 ⁻³	1090	39.4	63	203
GR9-17-4-1	Yes	No	1×10 ⁻³	1090	18.8	143	219
GR9-17-4-2	Yes	No	1×10 ⁻³	1090	17.6	151	214
GR9-17-4-3	Yes	No	1×10 ⁻³	1090	13.6	136	215
GR9-17-2-1	Yes	Yes	1×10 ⁻³	1090	16.6	109	215
GR9-17-2-2	Yes	Yes	1×10 ⁻³	1090	17.8	117	208
GR9-17-2-3	Yes	Yes	1×10 ⁻³	1090	18.4	98	210
K2-10-5-2	Yes	Yes	1×10 ⁻³	1090	14.4	114	199
K2-10-5-3	Yes	Yes	1×10 ⁻³	1090	19.3	109	210
#6, #23, #38 [12]	No	No	10	25	10.3	134	797
GR9-3-6-1	Yes	Yes	10	25	3.7	193	480
GR9-3-6-2	Yes	Yes	10	25	4.7	186	529
GR9-3-6-3	Yes	Yes	10	25	4.2	194	505
#8, #25, #40 [12]	No	No	10	750	33.8	95	489
GR9-15-5-1 ⁺	Yes	Yes	10	750	29.9	140	506
GR9-15-5-2	Yes	Yes	10	750	19.4	145	493
GR9-15-5-3	Yes	Yes	10	750	21.1	129	492
#9, #26, #41 [12]	No	No	10	900	29.5	83	396
GR9-17-1-1	Yes	Yes	10	900	20.3	133	433
GR9-17-1-2	Yes	Yes	10	900	10.4	141	387
GR9-17-1-3	Yes	Yes	10	900	13.7	120	395
#11, #27, #42 [12]	No	No	10	1090	37.0	79	313
GR9-17-3-1 ⁺	Yes	Yes	10	1090	28.0	130	334
GR9-17-3-2*	Yes	Yes	10	1090	23.0	139	318
GR9-17-3-3*	Yes	Yes	10	1090	21.7	121	326

*Specimen slightly curved after MRM heat treatment

⁺Fracture outside of fusion zone

⁺⁺Identical to the “corrected crosshead fracture strain”

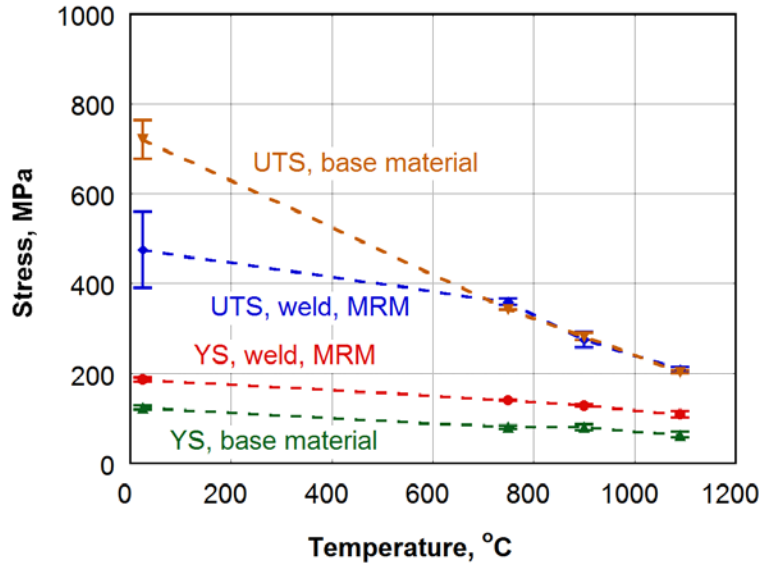


Fig. 15. Yield stress (YS) and ultimate tensile stress (UTS) for welded DOP-26 with MRM heat treatment deformed at a strain rate of $1 \times 10^{-3} \text{ s}^{-1}$. The YS and UTS values for the DOP-26 base material (without MRM heat treatment) from ORNL/TM-2007/81[12] are shown for comparison.

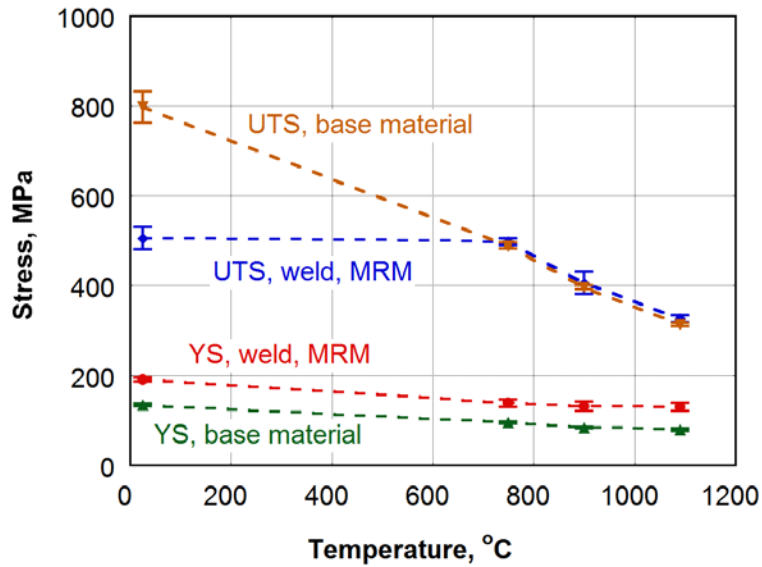


Fig. 16. Yield stress (YS) and ultimate tensile stress (UTS) for welded DOP-26 with MRM heat treatment deformed at a strain rate of 10 s^{-1} . The YS and UTS values for the DOP-26 base material (without MRM heat treatment) from ORNL/TM-2007/81[12] are shown for comparison.

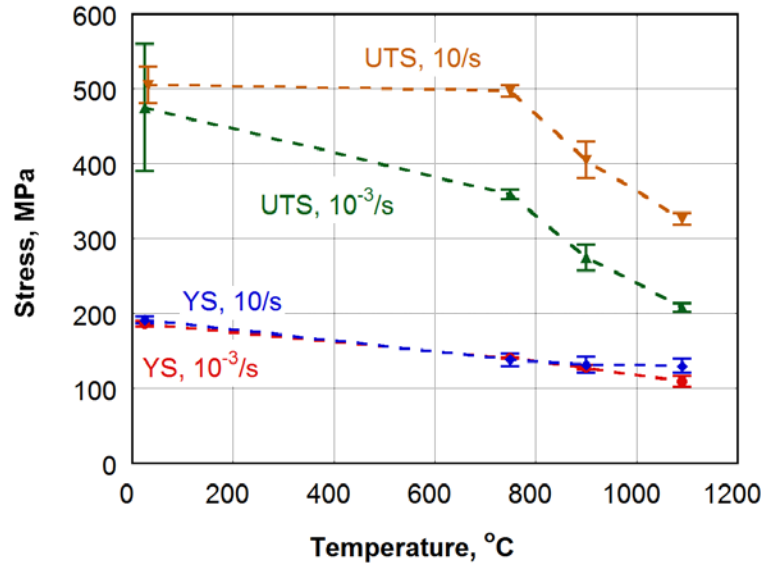


Fig. 17. Effect of strain rate on yield stress (YS) and ultimate tensile stress (UTS) of welded DOP-26 with MRM heat treatment.

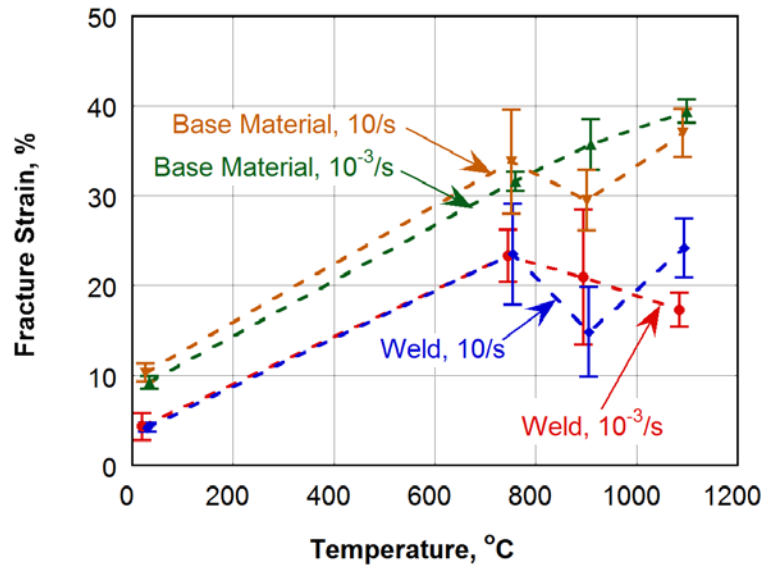


Fig. 18. Indent fracture strain of welded DOP-26 with MRM heat treatment. The corresponding values for the DOP-26 base material (without MRM heat treatment) are shown for comparison.

3.4. FRACTURE SURFACE OBSERVATIONS

An example of a room temperature fracture surface is shown in Fig. 19. This specimen exhibited a low fracture strain (2.9%) and no noticeable necking, consistent with sudden fracture at its UTS. Figure 20 shows the fracture surface of a specimen deformed at 900°C and $1 \times 10^{-3} \text{ s}^{-1}$. This specimen shows ductile fracture resulting in a necked, chisel-edge appearance consistent with the smooth and gradual decrease in the flow stress after the UTS has been reached. Figure 21 shows a cross section and the fracture surface of a specimen deformed at 900°C and 10 s^{-1} . Fracture occurred in the large-grained fusion zone of the weld. This particular specimen exhibited some necking, but fractured before it could draw out into a chisel-edge. Generally, when a specimen broke suddenly at the UTS, no necking or only a small amount of necking, occurred. When the stress decreased slowly beyond the UTS, significant necking was usually observed.

For those specimens that exhibited no significant necking, the fracture mode was analyzed in more detail. These specimens fractured usually in the large-grained fusion zone of the weld. In almost all cases the fracture was mostly intergranular, with only a few percent of transgranular fracture (Table 6). For improved ductility, it is desirable to shift the fracture mode, as much as possible, from intergranular to transgranular. It would be interesting to find out whether welds in the newly developed alloys microalloyed with both Th and Ce [1] would exhibit a larger fraction of transgranular failure than welds in DOP-26.

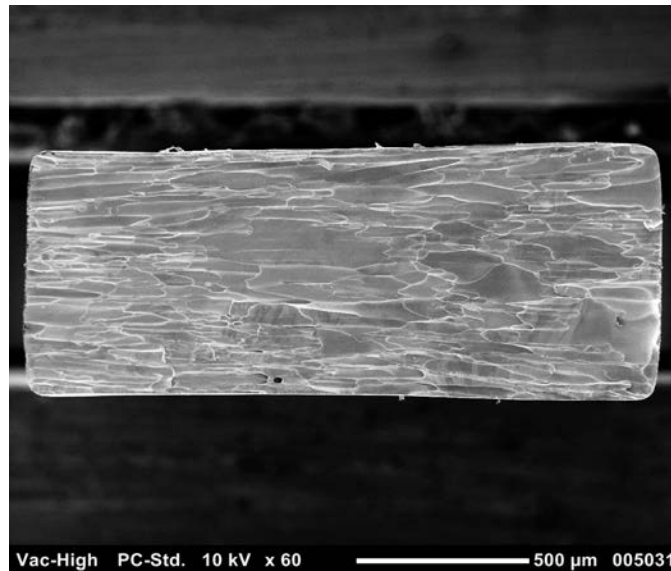


Fig. 19. Scanning electron microscope image of fracture surface of specimen GR9-3-5-1 tested at room temperature and $1 \times 10^{-3} \text{ s}^{-1}$.

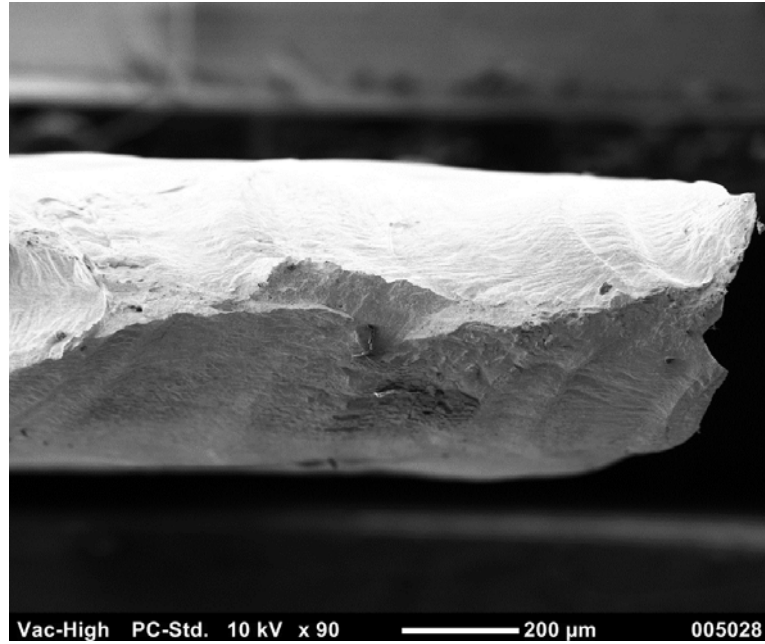


Fig. 20. Scanning electron microscope image of fracture surface of specimen GR9-3-7-3 tested at 900°C and $1 \times 10^{-3} \text{ s}^{-1}$.

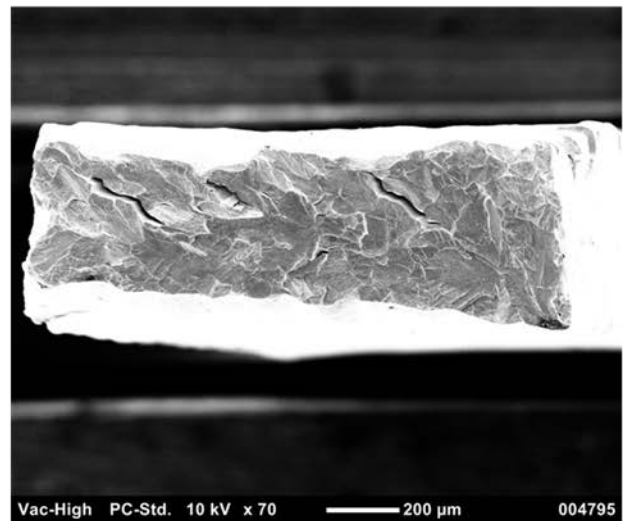
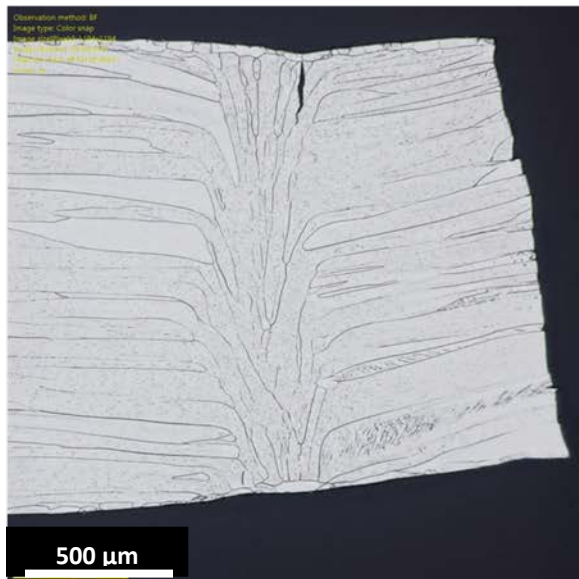


Fig. 21. Light microscope image of a longitudinal cross section (left) and scanning electron micrograph of the fracture surface (right) of specimen AR2-4-6-3 (a non-prime DOP-26 material) tested at 900°C and 10 s^{-1} .

Table 6. Percentage of Transgranular Failure on Fracture Surfaces of Welded DOP-26 with MRM Heat Treatment

ID	Strain Rate, s ⁻¹	Temperature, °C	Transgranular Fracture, %
GR9-3-5-1	1x10 ⁻³	25	0.8
GR9-3-5-2	1x10 ⁻³	25	2.5
GR9-3-5-3	1x10 ⁻³	25	3.1
GR9-3-6-1	10	25	1.0
GR9-3-6-2	10	25	3.2
GR9-3-6-3	10	25	2.0
GR9-15-5-1	10	750	78.2
GR9-15-5-2	10	750	11.8
GR9-15-5-3	10	750	9.9
GR9-17-1-1	10	900	5.5
GR9-17-1-2	10	900	4.5
GR9-17-1-3	10	900	26.9

4. SUMMARY AND CONCLUSIONS

The tensile properties of DOP-26 iridium specimens containing transverse welds were evaluated at temperatures ranging from room temperature to 1090°C and strain rates of 1×10⁻³ and 10 s⁻¹. The mechanical properties were compared to those of non-welded DOP-26 (the “base material” described in 2007 [12]). Depending on temperature and strain rate, the introduction of a weld increased the yield stress, and decreased the fracture strain, by up to a factor of ~2. Consistent with the reduction in the fracture strain, the presence of a weld reduced the UTS at room temperature significantly. At temperatures of 750°C and above, the UTS values of the welded and the base material agreed with each other. Increasing the strain rate from 1×10⁻³ s⁻¹ to 10 s⁻¹ did not increase the yield stress except at 1090°C. The UTS, on the other hand, increased strongly with increasing strain rate. Fracture occurred usually in the weld region. At lower temperatures and the higher strain rate fracture occurred with no or only little necking. In those cases, the fracture mode was mostly intergranular. Ductile failure accompanied by substantial necking was observed at 750°C and above for a strain rate of 1×10⁻³ s⁻¹, and at 1090°C for a strain rate of 10 s⁻¹. If the mechanical properties of the welds are determined to be a limitation, comparative work with improved iridium alloys, doped with both Th and Ce, would be worth pursuing.

5. SUGGESTIONS FOR FURTHER WORK

The present work shows, consistent with earlier work by Liu and David [13,14], that welding of DOP-26 increases the yield stress and lowers the tensile ductility. To better understand these findings and to improve the mechanical properties of the welds a number of experiments are suggested:

- nanoindentation measurements across the weld region and in the adjacent base material to determine where exactly the yield stress increase occurs; micropillar experiments would provide even more information,
- internal stress measurements after welding using X-ray or neutron diffraction,
- finite element simulations to determine whether, and to what extent, thermal contraction during the cool-down from welding can cause internal plastic deformation in the weld and the adjacent base material.
- texture measurements within the weld zone using X-ray or neutron diffraction. This would answer the question whether hard crystallographic orientations are present which would increase the yield stress,
- addressing the possibility of a yield stress increase in the base material due to constraints from a (hypothetically) stronger fusion zone,
- digital image correlation for room and high temperature tensile tests to determine localized deformation and strain accommodation across the weld region and the adjacent base material. This would help to identify the locations that are weak links leading to fracture,
- since fracture in welded DOP-26 is usually associated with the weld region it would be of interest to determine whether welds in newer alloys based on microalloying with Th plus Ce would have improved mechanical properties.

6. REFERENCES

- [1] E. P. George and C. T. Liu, *Micro- and Macro-Alloying of Ir-Base Alloys*, in Iridium (eds. E. K. Ohriner, R. D. Lanam, P. Panfilov, and H. Harada), The Minerals, Metals and Materials Society, Warrendale, PA, 2000, pp. 3-14.
- [2] C. T. Liu and H. Inouye, *Study of Iridium and Iridium-Tungsten Alloys for Space Radioisotopic Heat Sources*, Report ORNL-5240, Oak Ridge National Laboratory, Oak Ridge, Tennessee, December 1976.
- [3] C. T. Liu and H. Inouye, *Development and Characterization of an Improved Ir-0.3% W Alloy for Space Radioisotopic Heat Sources*, Report ORNL-5290, Oak Ridge National Laboratory, Oak Ridge, Tennessee, October 1977.
- [4] C. T. Liu, H. Inouye, and A. C. Schaffhauser, *Metallurgical and Mechanical Properties of Thorium-Doped Ir-0.3% W Alloys*, Report ORNL-5616, Oak Ridge National Laboratory, Oak Ridge, Tennessee, April 1980.
- [5] C. T. Liu, H. Inouye, and A. C. Schaffhauser, *Effect of Thorium Additions on Metallurgical and Mechanical Properties of Ir-0.3 pct W Alloys*, Metall. Trans. A, 12A (1981) 993-1002.
- [6] H. Inouye and C. T. Liu, *Iridium-Hafnium Alloy*, U.S. Patent 3,918,965, November 11, 1975.
- [7] C. L. White, R. E. Clausing, and L. Heatherly, *The Effect of Trace Element Additions on the Grain Boundary Composition of Ir + 0.3 pct W Alloys*, Metall. Trans. A, 10A (1979) 683-691.
- [8] T. G. George and M. F. Stevens, *The High-Temperature Impact Properties of DOP-26 Iridium*, JOM, 40 (Oct 1988) 32-35.
- [9] A. N. Gubbi, E. P. George, E. K. Ohriner, and R. H. Zee, *Influence of Cerium Additions on High-Temperature-Impact Ductility and Fracture Behavior of Iridium Alloys*, Metall. Mater. Trans. A, 28A (1997) 2049-2057.
- [10] E. P. George, C. G. McKamey, E. K. Ohriner, and E. H. Lee, *Deformation and Fracture of Iridium: Microalloying Effects*, Mater. Sci. Eng. A319-321 (2001) 466-470.
- [11] G. B. Ulrich, *Heat-Resistant Materials*, edited by K. Natesan and D. J. Tillack, ASM International, Materials Park, Ohio, 1991, pp. 187-195.
- [12] J. H. Schneibel, C. A. Carmichael and E. P. George, *High Strain Rate Tensile Testing of DOP-26 Iridium*, ORNL/TM-2007/81, November 2007.
- [13] C.T. Liu and S.A. David, *Welded Metal Grain Structure and Mechanical Properties of Iridium Alloy DOP-26*, ORNL-5857, August 1982.
- [14] C.T. Liu and S.A. David, *Weld Metal Grain Structure and Mechanical Properties of a Th-Doped Ir-0.3 pct W Alloy (DOP-26)*, Metall. Trans. A, 13A (1982)1043-1053.
- [15] Goodwin, G. M. 1987, *Development of a New Hot-Cracking Test – The Sigmajig*, Welding Journal, 66(2): 33S-38S).
- [16] T. Ishikawa, P.-F. Paradis, R. Fujii, Y. Saita, and S. Yoda, *Thermophysical Property Measurements of Liquid and Supercooled Iridium by Containerless Methods*, International Journal of Thermophysics, Vol. 26, No. 3, May 2005.
- [17] J. W. Arblaster, *Crystallographic Properties of Iridium – Assessment of Properties from Absolute Zero to the Melting Point*, Platinum Metals Rev., 2010, 54, (2), 93–102.

**APPENDIX A. WELDED IRIIDIUM ALLOY TENSILE TEST
SPECIMEN PREPARATION TRAVELER**

WELDED IRIIDIUM ALLOY TENSILE TEST SPECIMEN PREPARATION TRAVELER
for Welded Tensile Test Plan ORNL-WTT-TP4, Rev. 1 and Drawing: JHS-TENS-WELD-CB, Rev. 0

Blank Identity: _____

Step	Operations	Operator/Date
1 2525	Clean the blanks per procedure GPHS-Y-005 or equivalent.	
2 2525	Heat treat the blanks at 1375° ± 25° C for 1 h ± 10 min in a vacuum (≤ 1 x 10 ⁻⁴ torr) furnace dedicated for iridium use between iridium covers. Wrap in clean lens paper.	
3 2547	Weld at centerline parallel to blank rolling/grinding direction as described in Welded Tensile Test Plan: ORNL-WTT-TP4, Rev. 1 . Record order in campaign. ___ of ___	
4 2547	Scribe a mark on the blank (next to the weld on the top face) to show the start of the weld. Visually inspect welded blank at 10 to 25X magnification. Disregard areas within 9.5 mm (3/8 inches) of the blank edge. Measure weld face and root widths and weld thickness at approximately 1/3, 1/2 and 2/3 distance from the weld start. Weld Face width acceptance is 2 to 3 mm.	
	Weld Width, Face (mm)	
	Weld Width, Root (mm)	
	Weld Thickness (mm)	
	Full Penetration	<input type="checkbox"/> Yes <input type="checkbox"/> No <input type="checkbox"/> Yes <input type="checkbox"/> No <input type="checkbox"/> Yes <input type="checkbox"/> No
	Cracks, porosity, other observable defects	<input type="checkbox"/> Yes <input type="checkbox"/> No <input type="checkbox"/> Yes <input type="checkbox"/> No <input type="checkbox"/> Yes <input type="checkbox"/> No
5 7012	Wire electrical discharge machine (EDM) tensile specimens perpendicular to rolling/grinding direction oversize 0.25 mm (0.010 inches) as shown on drawing JHS-TENS-WELD-CB, Rev. 0 . Record the EDM wire used. Brand/type _____ Diam _____ Material _____	
6 7012	Scribe or laser mark specimen (3 tensile and 2 met) identities using blank number and specimen serial number per drawing.	
7 7012	Measure and record tensile specimen gage widths as EDM'ed. Specimen 1: W ₁ _____ W ₂ _____ W ₃ _____ Specimen 2: W ₁ _____ W ₂ _____ W ₃ _____ Specimen 3: W ₁ _____ W ₂ _____ W ₃ _____	
8 7012	Grind the tensile specimen removing 0.25 mm per side from specimen profile as shown on drawing and taper the gage section 0.025 mm (0.001 inches) from both ends to the middle. Record the grinding wheel and coolant used. Brand/type _____ Diam _____ Material _____ Coolant _____	
9 7012	Remove all grinding marks by polishing with the tensile specimen contour. Deburr and finish using 600 grit abrasive. Remove EDM layer on all edges at both grip ends using 320/400 grit and finishing with 600 grit abrasives.	
10 7012	Measure and record finished tensile specimen gage widths. Specimen 1: W ₁ _____ W ₂ _____ W ₃ _____ Specimen 2: W ₁ _____ W ₂ _____ W ₃ _____ Specimen 3: W ₁ _____ W ₂ _____ W ₃ _____	

WELDED IRIIDIUM ALLOY TENSILE TEST SPECIMEN PREPARATION TRAVELER
for Welded Tensile Test Plan ORNL-WTT-TP4, Rev. 1 and Drawing: JHS-TENS-WELD-CB, Rev. 0

11 7012	Grind or hand polish the met specimen edges to visually remove the residual EDM layer from the EDM/weld edges.															
12 7012	Individually bag and tag each specimen and separately bag and tag each blank skeleton. Return to G. B. Ulrich/B. R. Friske.															
13 4500S	<p>Metallographically evaluate welded remnant. (optional) Identity _____</p> <p>Record the number of weld grains through thickness at each distance from weld centerline (mm)</p> <table border="1" style="width:100%; border-collapse: collapse;"> <tr> <td style="width:14.28%;">-2</td> <td style="width:14.28%;">-1.2</td> <td style="width:14.28%;">-0.6</td> <td style="width:14.28%;">0</td> <td style="width:14.28%;">0.6</td> <td style="width:14.28%;">1.2</td> <td style="width:14.28%;">2.0</td> </tr> <tr> <td> </td> </tr> </table> <p>Any weld grain \geq 50% of weld thickness at any location <input type="checkbox"/> Yes <input type="checkbox"/> No</p> <p>Min. of 6 weld grains through weld thickness at specified locations <input type="checkbox"/> Yes <input type="checkbox"/> No</p> <p>Cracks, porosity, other observable defects <input type="checkbox"/> Yes <input type="checkbox"/> No</p>	-2	-1.2	-0.6	0	0.6	1.2	2.0								
-2	-1.2	-0.6	0	0.6	1.2	2.0										
14 CAC	Verify all tensile specimen surfaces, especially gauge and grip sections, are properly polished. Re-polish, if necessary.															
15 5500	Ultrasonically inspect tensile specimens. (optional)															
16 2547	Dimensionally inspect tensile specimens (including surface profilometry, if directed to do so, of both gauge section edges). Visually inspect surfaces for slivers, burrs, fissures, seams, blisters, cracks, and extraneous matter using fluorescent lighting and 20X magnification, however, magnification up to 50X may be used to identify/clarify features observed at 20X. Notify Engineer of non-conforming attributes for possible rework.															
17 2525	<p>Clean the tensile specimens per procedure GPHS-Y-005 or equivalent. Weigh tensile specimen and record weight to the nearest 0.0001 g.</p> <p>Specimen 1: _____ g Specimen 2: _____ g Specimen 3: _____ g</p>															
18 2525	Heat treat the tensile specimens at $1140^{\circ} \pm 25^{\circ} \text{ C}$ for $1176 \text{ h} \pm 10 \text{ h}$ in a vacuum ($\leq 1 \times 10^{-4}$ torr) furnace with a graphite hot zone. Place the specimens between iridium covers. After the heat treatment wrap the specimens in clean lens paper. (optional)															
19 CAC	<p>Using clean gloves and clean tooling surfaces, mark tensile specimens with Vickers microindentation hardness marks along the centerline of the full gauge section spaced approximately 0.89 mm (0.035 inches) apart using a load of 1000 gf. Record spacing between indentations. Tensile specimens may be re-cleaned per procedure GPHS-Y-005 or equivalent if cleanliness is compromised. Note/record if re-cleaned.</p> <p>Specimen 1: _____ Specimen 2: _____ Specimen 3: _____</p>															
20 CAC	Test per ORNL-WTT-TP4, Rev. 1															